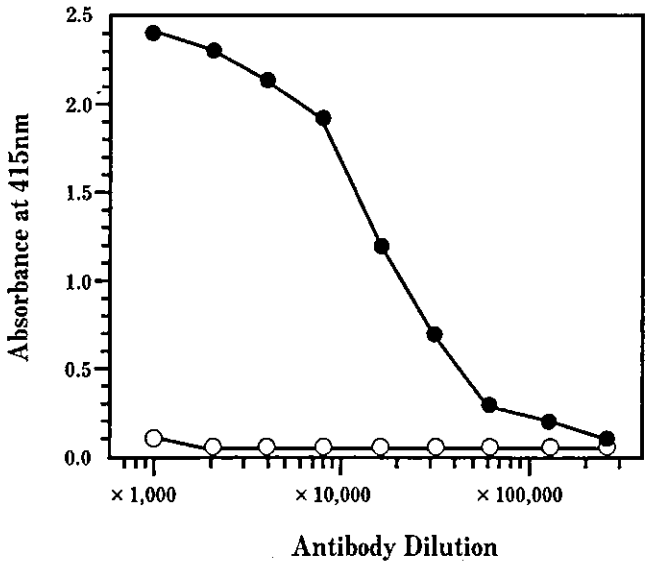

Fig. 1 Specificity of antibody against Prx2. The immunoreactivity of the antibody to HSA-conjugated Prx2 peptide (*solid circles*) and native HSA (*open circles*) was determined by noncompetitive ELISA. The anti-Prx2 antibody recognizes the HSA-conjugated Prx2 peptide, but does not react with HAS (*Prx2* peroxiredoxin2, *ELISA* enzyme-linked immunosorbent assay, *HAS* human serum albumin)

Histochemical and immunohistochemical studies were also carried out on specimens from transgenic rats with the H46R and G93A types of mutations (three rats of each type). The H46R rats used in this study were a transgenic line (H46R-4) in which the level of human SOD1 with the H46R mutation was 6 times the level of that of endogenous rat SOD1 [27]. The G93A rats were a transgenic line (G93A-39) in which the level of human SOD1 with the G93A mutation was 2.5 times the level of endogenous rat SOD1 [27]. These rats were killed at an age of over 180 days; an age corresponding to an advanced stage of disease in these strains. The detailed clinical signs and pathological characteristics of the neuronal LBHIs of the H46R and G93A rats have been demonstrated previously [27]. As rat controls, we investigated the spinal cord specimens of three age-matched littermates of H46R and G93A rats and five age-matched normal Sprague-Dawley rats. Rats were anesthetized with sodium pentobarbital (0.1 ml/100 g body weight). After perfusion of the rats via the aorta with physiological saline at 37°C, they were fixed by perfusion with 4% paraformaldehyde in 0.1 M cacodylate buffer (pH 7.3). The spinal cords were removed and then postfixed in the same solution.

Histochemistry and immunohistochemistry

After fixation, the specimens were embedded in paraffin, cut into 6-μm-thick sections, and examined by light microscopy. Spinal cord sections were stained by the following histochemical methods: hematoxylin and eosin (HE), Klüver-Barrera, Holzer, phosphotungstic acid-hematoxylin, periodic acid-Schiff, alcian blue, Masson's trichrome, Mallory azan and Gallyas-Braak stains. Representative paraffin sections were used for immunohistochemical assays. The following primary antibodies were utilized: an affinity-purified rabbit antibody against Prx2 (concentration: 1 μg/ml), a polyclonal antibody to GPx1 [diluted 1:2,000 in 1% bovine serum albumin-containing phosphate-buffered saline (BSA-PBS), pH 7.4] [2], and a polyclonal antibody to human SOD1 (diluted 1:10,000 in 1% BSA-PBS, pH 7.4) [1]. Sections were deparaffinized, and endogenous peroxidase activity was quenched by incubation for 30 min with 0.3% H_2O_2. The sections were then washed in PBS. Normal sera homologous with secondary antibody was used as a blocking reagent. Tissue sections were incubated with the primary antibodies for 18 h at 4°C. PBS-exposed sections served as controls. As a preabsorption test, some sections were incubated with the anti-Prx2 antibody that had been preabsorbed with an excess amount of the synthetic Prx2 peptide. Bound antibodies were visualized by the avidin-biotin-immunoperoxidase complex (ABC) method using the appropriate Vectastain ABC Kit (Vector Laboratories, Burlingame, CA) and 3,3'-diaminobenzidine tetrahydrochloride (DAB; Dako, Glostrup, Denmark) as chromogen.

Results

We successfully produced an affinity-purified rabbit antibody against Prx2 peptide (amino acids 184–198; although this amino acid sequence is homologous with that of each C-terminal region of the human, rat, mouse, Chinese hamster or Bos Taurus Prx2, this peptide does not share homology with other members of the Prx family or any other peptide sequence in GenomeNet), and applied it to stain of paraffin sections from both humans and rats. This anti-Prx2 antibody recognized the HSA-conjugated Prx2 peptide, but did not react with HSA (Fig. 1).

Analysis of the essential changes of five cases of FALS revealed a subtype of FALS with posterior column involvement (PCI). This subtype is characterized by the degeneration of the middle root zones of the posterior column, Clarke nuclei, and the posterior spinocerebellar tracts, in addition to spinal cord motor neuron lesions. A long-term surviving patient with a clinical course of 11 years

Table 1 Characteristics of five FALS cases (*FALS* familial amyotrophic lateral sclerosis, *SOD* superoxide dismutase, *LBHI* Lewy body-like hyaline inclusion, *2-bp* two-base pair, *PCI* posterior column involvement type, + detected, *ND* not determined, *As* asphyxia, *IH* intraperitoneal hemorrhage, *RD* respiratory distress, *Pn* pneumonia)

Case	Age (years)	Sex	Cause of Death	FALS Duration	SOD1 mutation	FALS subtype	Neuronal LBHI
Japanese Oki family							
1	46	F	As	18 months	2-bp deletion (126)	PCI	+
2	65	M	IH	11 years	2-bp deletion (126)	PCI and degeneration of other systems	+
American C family							
3	39	M	RD	7 months	A4V	PCI	+
4	46	M	Pn	8 months	A4V	PCI	+
5	66	M	Pn	1 year	ND	PCI	+

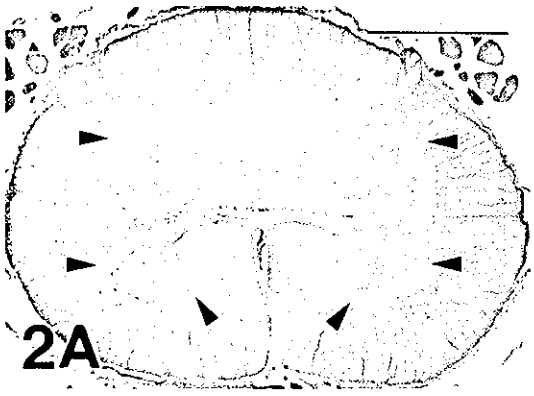
2A

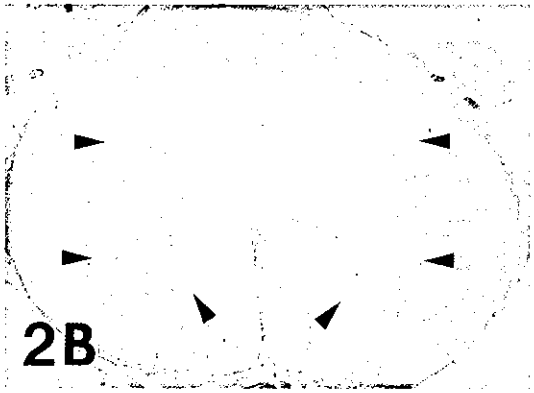
2B

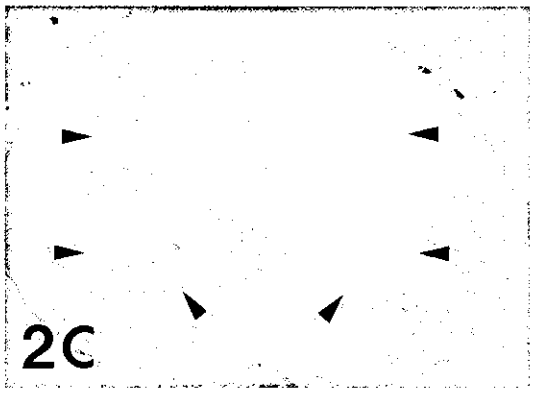
2C


3A


3C

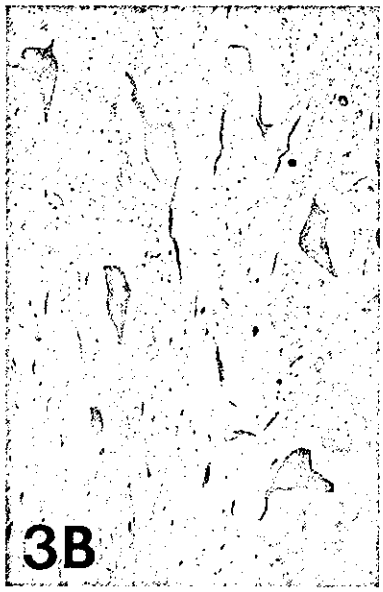
3B


3D


3E

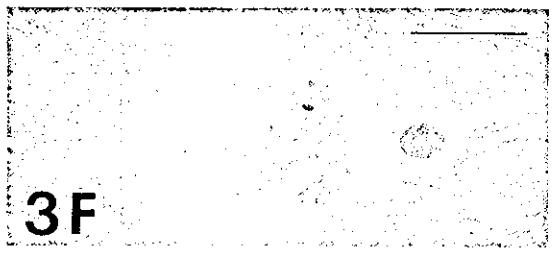
3F

◀ Fig. 2 Serial transverse sections through the lumbar segments of the normal human spinal cords. A Light microscopic preparation stained with HE. B, C Immunostaining for GPx1 (B) and Prx2 (C). GPx1 and Prx2 immunoreactivities are found diffusely in the neuropil with considerably less intensity (*arrowheads*). No counterstaining (*HE* hematoxylin and eosin, *GPx1* glutathione peroxidase1, *Prx2* peroxiredoxin2). *Bar* A (also for B, C) 2 mm

Fig. 3 Detection of Prx2 and GPx1 in the normal motor neurons of the human spinal cord. A–D Serial sections. A Staining with HE. B Immunostaining with the antibody against GPx1, showing GPx1-positive neurons. C Immunostaining with the antibody to Prx2. Immunoreactivity is identified in most of the neurons. Thus, most of the normal motor neurons in the spinal cord co-express both GPx1 (B) and Prx2 (C), although their staining intensities in neurons vary. D Immunostaining with anti-Prx2 antibody pretreated with an excess of the synthetic Prx2 peptide. No immunoreaction products are observed in the motor neurons and neuropil. E GPx1 immunostaining of the neuronal cytoplasm and proximal dendrites is observed, but no intranuclear localization is seen. F Prx2 immunostaining of the neuronal cytoplasm and proximal dendrites is observed, and a nucleus of the neuron is also immunostained by the anti-Prx2 antibody. B–F No counterstaining (*HE* hematoxylin and eosin, *GPx1* glutathione peroxidase1, *Prx2* peroxiredoxin2). *Bars* A (also for B–D) 100 μm; E, F 50 μm

(case 2 in Table 1) showed multisystem degeneration in addition to the features of FALS with PCI. Neuronal Lewy body-like hyaline inclusions (LBHIs) were present in all five FALS cases. As observed in HE preparations, the neuronal LBHIs in the FALS patients were essentially identical to those in the H46R and G93A transgenic rats; the inclusions were round eosinophilic or paler inclusions and often showed eosinophilic cores with pale peripheral halos. In mutant SOD1-linked FALS patients, the neuronal LBHIs were generally composed of eosinophilic cores with pale peripheral halos and sometimes showed ill-defined forms that consisted of obscure eosinophilic materials. In H46R and G93A transgenic rats, the intracytoplasmic LBHIs with cores and halos were less frequently observed and round or sausage-like LBHIs, which were though to be intradendritic LBHIs, were often seen in the neuropil, although these round or sausage-like LBHIs in the neuropil were not remarkable in the human FALS patients. Histochemically, most of the neuronal LBHIs in the H46R and G93A transgenic rats were argyrophilic in Gallyas-Braak stain, and they were generally blue to violet after Masson's trichrome or Mallory azan staining, similar to the histochemical findings of the neuronal LBHIs of the human FALS patients. The spinal cords of normal individuals in both humans and rats did not exhibit any distinct histopathological alterations.

When control and representative paraffin sections were incubated with PBS alone (i.e., no primary antibody), no staining was detected. Prx2 immunoreactivity in normal spinal cords was identified in almost all neurons. In addition, Prx2-immunostaining was found throughout the neuropil with considerably lower intensity (Fig. 2A, C). With respect to the intracellular localization of Prx2, immunostaining of the neuronal cytoplasm and proximal dendrites was specifically observed (Fig. 3A, C). Additionally, the nuclei of some neurons were immunostained by the anti-Prx2 antibody, albeit the staining of positively stained nuclei varied (Fig. 3F). Incubation of sections with anti-Prx2 antibody that had been pretreated with an excess of the synthetic Prx2 produced no staining (Fig. 3D).

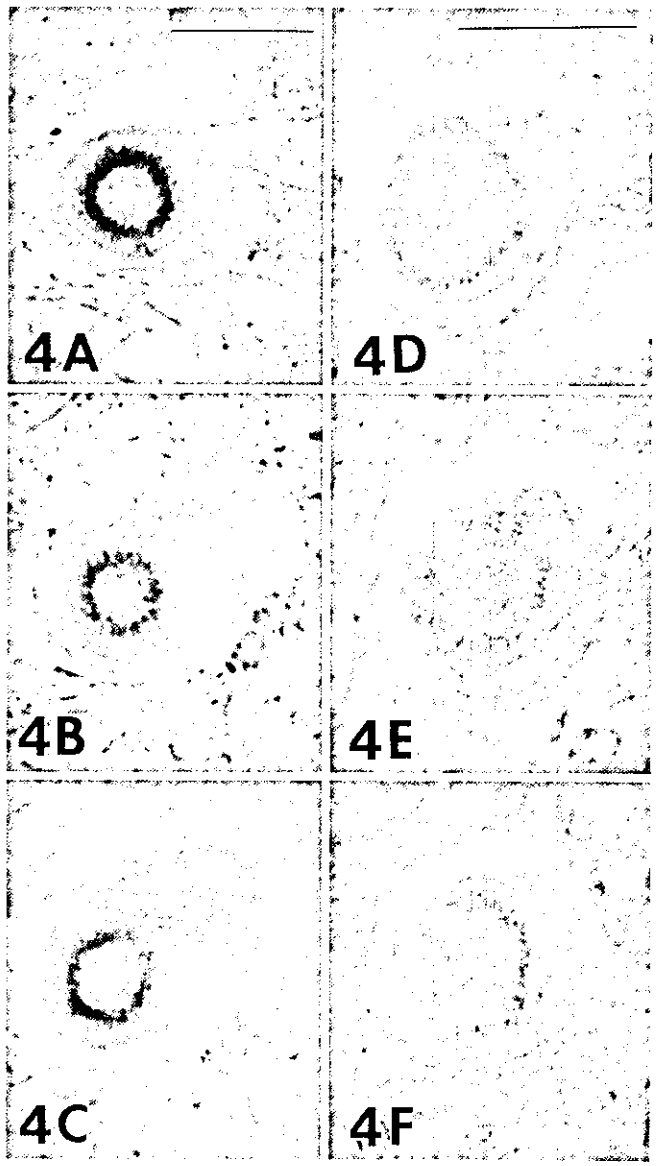

Fig. 4A–C Serial sections of a typical LBHI with a core and halo in neurons from the spinal cord of an FALS patient with a two-base pair deletion in the SOD1 gene. A Immunostaining for SOD1: immunoreactivity is mostly restricted to the halo. B Immunostaining for GPx1: immunoreactivity is located in the SOD1-positive portion of the LBHI. C Immunoreactivity for Prx2. Co-localization of the three proteins SOD1, GPx1 and Prx2 in the LBHI is evident. D–F Serial sections of a core and halo-type LBHI in a transgenic rat expressing human SOD1 with an H46R mutation. Immunostaining for SOD1 (D), GPx1 (E) and Prx2 (F). Similar stainability and immunolocalization of SOD1, GPx1 and Prx2 in the LBHI are observed (*LBHI* Lewy body-like hyaline inclusion, *FALS* familial amyotrophic lateral sclerosis, *SOD1* superoxide dismutase 1, *GPx1* glutathione peroxidase1, *Prx2* peroxiredoxin2). A–F No counterstaining. *Bars* A (also for B, C), D (also for E, F) 25 μm

A neuropil staining pattern similar to that for Prx2 was observed with GPx1; weak GPx1 immunoreactivity was diffusely seen in the neuropil in transverse sections of the

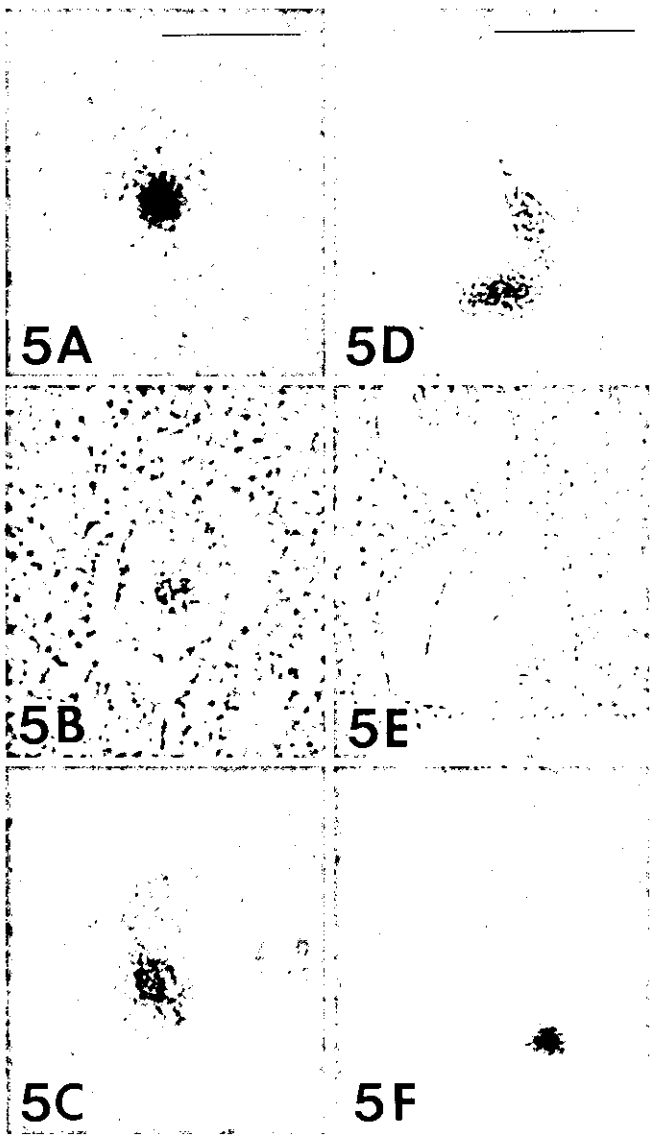

Fig. 5A–C Serial sections of an LBHI in an FALS patient with an A4V mutation in SOD1 gene. Immunostaining for SOD1 (**A**), GPx1 (**B**) and Prx2 (**C**). Co-localization of the three proteins in the LBHI is mainly observed in the core (**A–C**). **D–F** Serial sections of an LBHI in an FALS patient with a two-base pair deletion in the SOD1 gene. Immunostaining for SOD1 (**D**), GPx1 (**E**) and Prx2 (**F**). Immunostaining GPx1 (**E**) and Prx2 (**F**) are observed in only part of the SOD1-positive LBHI. The precise intra-inclusional immunolocalizations of these three proteins differ from each other in this LBHI (*LBHI* Lewy body-like hyaline inclusion, *FALS* familial amyotrophic lateral sclerosis, *SOD1* superoxide dismutase 1, *GPx1* glutathione peroxidase1, *Prx2* peroxiredoxin2). *Bars* **A** (also for **B**, **C**), **D** (also for **E**, **F**) 25 μm

spinal cords (Fig. 2A, B). GPx1 immunostaining was observed in the cytoplasm with cell bodies and proximal dendrites being essentially identified (Fig. 3A, B, E), but no intranuclear staining was observed (Fig. 3B, E). The stainability and intensity of Prx2 and GPx1 in the normal anterior horn cells of the spinal cords in humans were identical to those in rats. Therefore, almost all of the normal motor neurons in the spinal cords co-expressed both Prx2 and GPx1 (Fig. 3A–C), although the staining intensities of positively stained neurons varied.

Corroborating recent findings [12, 13, 16, 19, 27, 30], almost all of the neuronal LBHIs in both the FALS patients from two different families and races (Japanese Oki family and American C family) and the transgenic rats expressing two different human SOD1 mutations (H46R and G93A) were intensely immunostained by the antibody against human SOD1 (Figs. 4A, D; 5A, D; 6A; 7A). Most neuronal LBHIs were also immunoreactive for Prx2, although the intensity of Prx2 immunoreactivity in the LBHIs varied (Figs. 4C, F; 5C, F; 6B). The LBHIs in the neurons of the FALS patients and transgenic rats (H46R and G93A) showed a similar immunoreactivity for Prx2. The Prx2 immunolocalization in many intracytoplasmic and intraneuritic LBHIs was similar to that of SOD1 in both diseases. In core and halo-type LBHIs, the reaction product deposits of the antibody against Prx2 were generally restricted to the periphery (Fig. 4C, F), and were sometimes localized in the cores alone (Fig. 5C). In ill-defined LBHIs, Prx2 immunostaining was distributed throughout each inclusion. In some inclusions, however, expression of Prx2 was observed in only part of the inclusion (Fig. 5F). With respect to the GPx1 immunostaining in the neuronal LBHIs, similar stainability and immunolocalization to Prx2 were confirmed in the core and halo types as well as the ill-defined forms; most LBHIs in neurons were immunostained by the anti-GPx1 antibody with various intensities (Figs. 4B, E; 5B, E; 7B). The immunoreactivity for GPx1 in the FALS patients was similar to that in the transgenic rats (H46R and G93A). Like Prx2, the immunolocalization of GPx1 was similar to that of SOD1 in both diseases. GPx1-immunoreactive products in many core and halo-type inclusions were mainly localized in the periphery portions (Fig. 4B, E), but sometimes in the core portions alone (Fig. 5B). In some inclusions, the reaction products were confined to certain regions of each inclusion (Fig. 5E).

Noticeably, the co-localization of the three proteins SOD1, Prx2 and GPx1 in neuronal LBHIs in SOD1-mutated FALS patients and transgenic rats (H46R and G93A) was evident (Figs. 4, 5, 6, 7), although all three immunoreactive intensities varied. With respect to the intra-inclusional localization, many inclusions showed similar co-localizations of these three proteins (Figs. 4, 5A–C). In some LBHIs, the precise intra-inclusional immunolocalizations of the three proteins differed: Prx2 (Fig. 5D, F) and GPx1 (Fig. 5D, E) immunostaining was observed in only some areas of the SOD1-positive LBHIs.

Discussion

Under normal physiological conditions, Prx2 and GPx1 immunoreactivities in the spinal cord anterior horns in humans and rats are primarily identified in the neurons: cytoplasmic staining with both antibodies is observed in almost all of the anterior horn cells. Like Prx1 [26, 33], intranuclear localization in some neurons is also observed in Prx2 immunostaining. Considering that endogenous Prx2

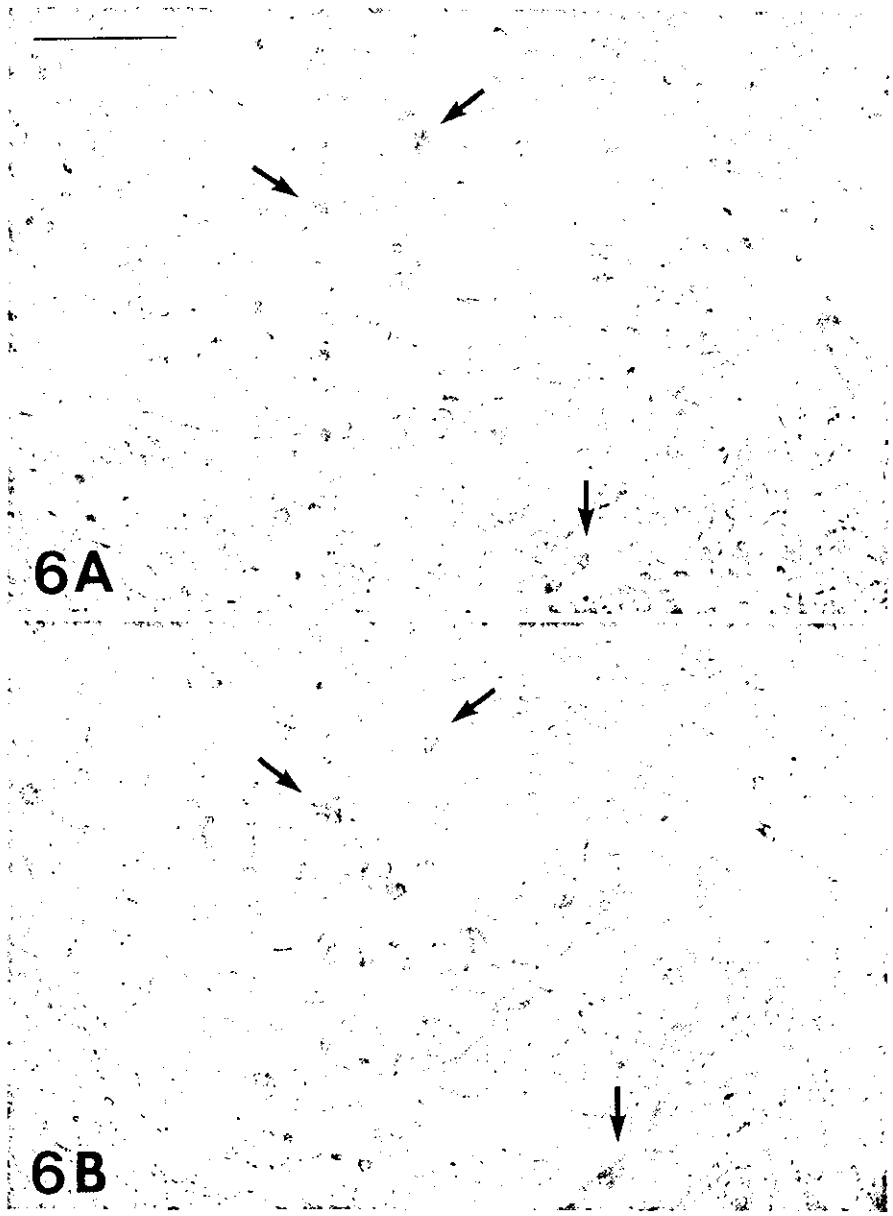

Fig. 6 Serial sections of the spinal anterior horn in a transgenic rat expressing human SOD1 with an H46R mutation immunostained with antibodies against SOD1 (**A**) and Prx2 (**B**). Round and sausage-like LBHIs in the neuropil are positive for both SOD1 and Prx2 (*arrows*) (*SOD1* superoxide dismutase1, *LBHI* Lewy body-like hyaline inclusion, *Prx2* peroxiredoxin2). *Bar* **A** (also for **B**) 50 μm

and GPx1 within the neuronal cytoplasm are extremely effective regulators of the redox system, our immunohistochemical finding that almost all of the normal spinal motor neurons co-expressed both Prx2 and GPx1 confirms that these motor neurons maintain themselves using the intracellular Prx2/GPx1 system, that is, the redox system.

As expected [12, 13, 16, 27, 30], SOD1 protein (probably the mutant form) was found to aggregate in the anterior horn cells as neuronal LBHIs in FALS patients with SOD1 gene mutations and transgenic rats expressing human SOD1 with H46R and G93A mutations. Intense co-expression of SOD1, Prx2, and GPx1 in neuronal LBHIs in both diseases was evident. To eliminate ROSs, SOD1-mutated motor neurons in mutant SOD1-linked FALS and transgenic rats (G46R and G93A) induce mutant/wild-type SOD1 as an antioxidant system and Prx2/GPx1 as a redox system. In this in vivo milieu where mutant SOD1 exists, Prx2 and GPx1 would aberrantly interact with the mutant SOD1, which is assumed to aggregate easily by itself [8]. Among the multiple theories of how mutant SOD1 contributes to motor neuron death in mutant SOD1-related FALS and transgenic animal models expressing human mutant SOD1, the aggregation of mutant SOD1 in neurons leads to part of the mutant SOD1-mediated toxicity through the formation of advanced glycation endproduct-modified SOD1 that is insoluble and cytotoxic [16]. Our recent study of FALS patients with a two-base pair deletion at codon 126 of the SOD1 gene (Oki family) and G85R transgenic mice has revealed that not only does mutant SOD1 provoke inclusion formation, but that normal SOD1 also co-aggregates in these inclusions [3]. Together with the facts that there are neuronal LBHIs positive for

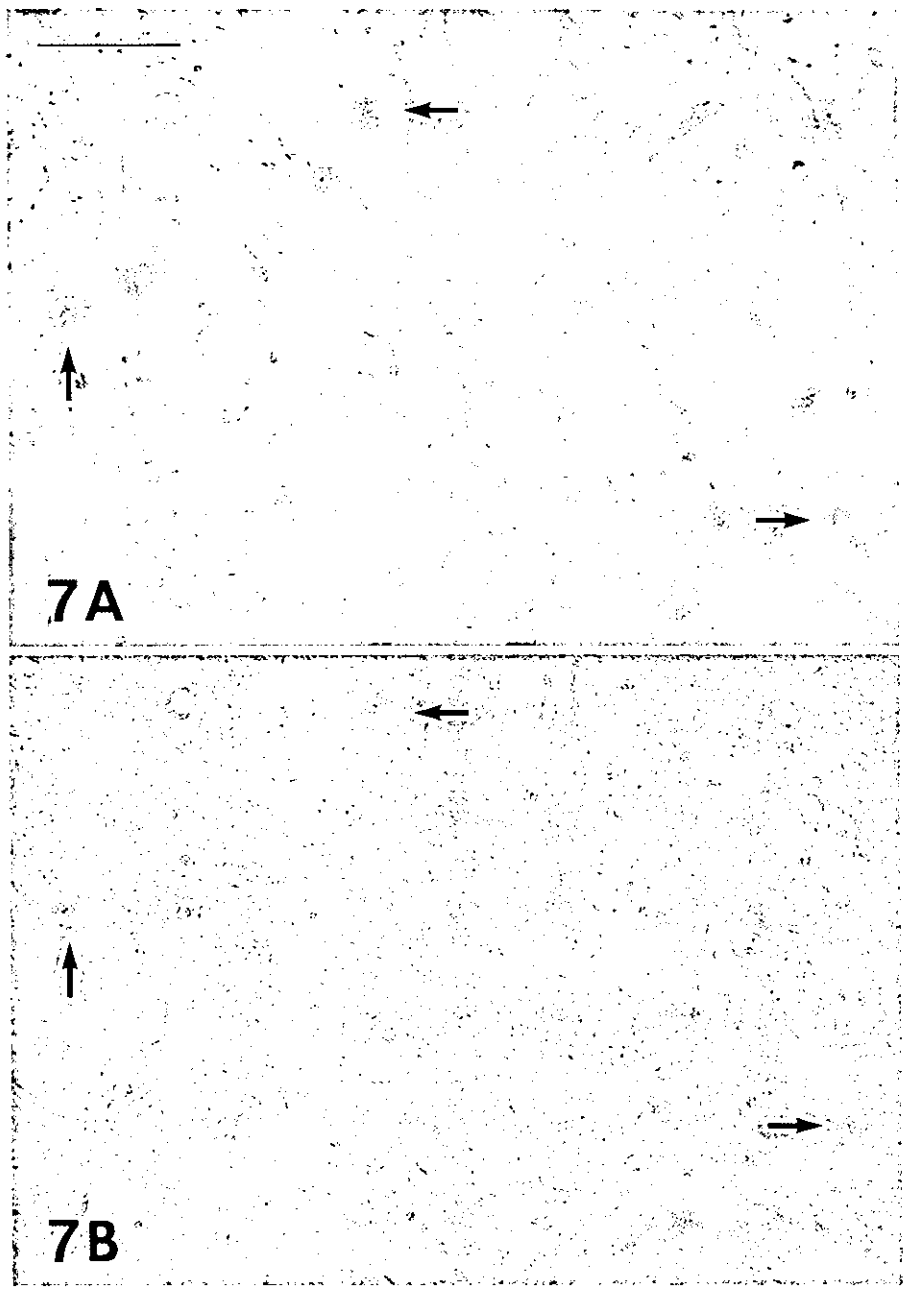

Fig. 7 Serial sections of the spinal anterior horn in a transgenic rat expressing human SOD1 with an H46R mutation immunostained with antibodies against SOD1 (**A**) and GPx1 (**B**). Round LBHIs in the neuropil are positive for both SOD1 and GPx1 (*arrows*) (*SOD1* superoxide dismutase1, *LBHI* Lewy body-like hyaline inclusion, *GPx1* glutathione peroxidase1). *Bar* **A** (also for **B**) 50 μm

SOD1, Prx2, and GPx1 in the milieu where mutant SOD1 exists but no LBHIs (no aggregations) exist under physiological conditions, our study demonstrates an aberrant interaction of Prx2/GPx1 with mutant SOD1, the aggregation of which results in neuronal LBHIs. In addition, intra-inclusional co-aggregation of Prx2/GPx1 with mutant SOD1 causes the intracytoplasmic reduction of Prx2/GPx1, thereby reducing the availability of the redox system. A similar aberrant interaction of the copper chaperone for SOD (CCS) and SOD1 (probably CCS-mutant SOD1) also occurs in the formation of the neuronal LBHIs in mutant SOD1-linked FALS [19] and the mutant SOD1 transgenic mouse model [32]. Such sequestration into LBHIs has also been observed for normal cytosolic constitutive proteins including tubulin and tau protein, as well as neuron-specific constitutive proteins containing phosphorylated neurofilament proteins (NFP), nonphosphorylated NFP, synaptophysin, and neuron-specific enolase [13, 17, 18]; this results in partial impairment of the maintenance of cell metabolism [13, 17, 18]. Although we cannot readily compare the sequestration of normal constitutive proteins with the aberrant interaction of cytotoxic mutant SOD1 with Prx2/GPx1 directly regulating a redox system, our finding leads us to speculate that not only co-aggregation of Prx2/GPx1 and SOD1 into LBHIs, but also intracytoplasmic reduction of Prx2/GPx1 in both diseases may partly contribute to the breakdown of the redox system itself in these SOD1-mutated neurons, and this may be one of the

endogenous mechanisms that accelerate neuronal death. This hypothesis would appear to be compatible with the aggregation toxicity theory. It remains to be determined whether this aberrant interaction of Prx2/GPx1 with mutant SOD1 is a direct or an indirect effect based on the pathogenesis of SOD1-mutated FALS disease itself or whether Prx2 and GPx1 play a primary or a secondary role to mutant SOD1. Consequently, we would like to emphasize that the aberrant interaction and co-aggregation of Prx2/GPx1 and SOD1 (probably Prx2/GPx1 and mutant SOD1) in FALS patients with SOD1 gene mutations and transgenic rats expressing human SOD1 mutations may amplify a more marked mutant SOD1-mediated toxicity.

Acknowledgements This study was supported in part by a Grant-in-Aid for Scientific Research (c) (2) from the Ministry of Education, Culture, Sports, Science and Technology of Japan (S.K.: 13680821) and by a Grant from the Ministry of Health, Labour and Welfare of Japan (S.K. and Y.I.).

References

1. Asayama K, Burr IM (1984) Joint purification of mangano and cuprozinc superoxide dismutases from a single source: a simplified method. Anal Biochem 136:336–339
2. Asayama K, Yokota S, Dobashi K, Hayashibe H, Kawaoi A, Nakazawa S (1994) Purification and immunoelectron microscopic localization of cellular glutathion peroxidase in rat hepatocytes: quantitative analysis by postembedding method. Histochemistry 102:213–219
3. Bruijn LI, Houseweart MK, Kato S, Anderson KL, Anderson SD, Ohama E, Reaume AG, Scott RW, Cleveland DW (1998) Aggregation and motor neuron toxicity of an ALS-linked SOD1 mutant independent from wild-type SOD1. Science 281: 1851–1854
4. Chae HZ, Kim IH, Kim K, Rhee SG (1993) Cloning, sequencing, and mutation of thiol-specific antioxidant gene of *Saccharomyces cerevisiae*. J Biol Chem 268:16815–16821
5. Chae HZ, Chung SJ, Rhee SG (1994) Thioredoxin-dependent peroxide reductase from yeast. J Biol Chem 269:27670–27678
6. Chae HZ, Robison K, Poole LB, Church G, Storz G, Rhee SG (1994) Cloning and sequencing of thiol-specific antioxidant from mammalian brain: alkyl hydroperoxide reductase and thiol-specific antioxidant define a large family of antioxidant enzymes. Proc Natl Acad Sci USA 91:7017–7021
7. De Haan JB, Bladier C, Griffiths P, Kelner M, O'Shea RD, Cheung NS, Bronson RT, Silvestro MJ, Wild S, Zheng SS, Beart PM, Hertzog PJ, Kola I (1998) Mice with a homozygous null mutation for the most abundant glutathione peroxidase, Gpx1, show increased susceptibility to the oxidative stress-inducing agents paraquat and hydrogen peroxide. J Biol Chem 273:22528–22536
8. Durham HD, Roy J, Dong L, Figlewicz DA (1997) Aggregation of mutant Cu/Zn superoxide dismutase proteins in a culture model of ALS. J Neuropathol Exp Neurol 56:523–530
9. Fridovich I (1986) Superoxide dismutases. Adv Enzymol Relat Area Mol Biol 58:61–97
10. Jin D-Y, Chae HZ, Rhee SG, Jeang K-T (1997) Regulatory role for a novel human thioredoxin peroxidase in NF-kappaB activation. J Biol Chem 272:30952–30961
11. Kato S, Shimoda M, Morita T, Watanabe Y, Nakashima K, Takahashi K, Ohama E (1996) Neuropathology of familial ALS with a mutation of the superoxide dismutase I gene. In: Nakano I, Hirano A (eds) Amyotrophic lateral sclerosis: progress and perspectives in basic research and clinical application. Elsevier Science, Amsterdam, pp 117–122
12. Kato S, Shimoda M, Watanabe Y, Nakashima K, Takahashi K, Ohama E (1996) Familial amyotrophic lateral sclerosis with a two base pair deletion in superoxide dismutase 1 gene: multisystem degeneration with intracytoplasmic hyaline inclusions in astrocytes. J Neuropathol Exp Neurol 55:1089–1101
13. Kato S, Hayashi H, Nakashima K, Nanba E, Kato M, Hirano A, Nakano I, Asayama K, Ohama E (1997) Pathological characterization of astrocytic hyaline inclusions in familial amyotrophic lateral sclerosis. Am J Pathol 151:611–620
14. Kato S, Horiuchi S, Nakashima K, Hirano A, Shibata N, Nakano I, Saito M, Kato M, Asayama K, Ohama E (1999) Astrocytic hyaline inclusions contain advanced glycation endproducts in familial amyotrophic lateral sclerosis with superoxide dismutase 1 gene mutation: immunohistochemical and immunoelectron microscopical analyses. Acta Neuropathol 97: 260–266
15. Kato S, Saito M, Hirano A, Ohama E (1999) Recent advances in research on neuropathological aspects of familial amyotrophic lateral sclerosis with superoxide dismutase 1 gene mutations: neuronal Lewy body-like hyaline inclusions and astrocytic hyaline inclusions. Histol Histopathol 14:973–989
16. Kato S, Horiuchi S, Liu J, Cleveland DW, Shibata N, Nakashima K, Nagai R, Hirano A, Takikawa M, Kato M, Nakano I, Ohama E (2000) Advanced glycation endproduct-modified superoxide dismutase-1 (SOD1)-positive inclusions are common to familial amyotrophic lateral sclerosis patients with SOD1 gene mutations and transgenic mice expressing human SOD1 with G85R mutation. Acta Neuropathol 100:490–505
17. Kato S, Takikawa M, Nakashima K, Hirano A, Cleveland DW, Kusaka H, Shibata N, Kato M, Nakano I, Ohama E (2000) New consensus research on neuropathological aspects of familial amyotrophic lateral sclerosis with superoxide dismutase 1 (SOD1) gene mutations: inclusions containing SOD1 in neurons and astrocytes. Amyotroph Lateral Scler Other Motor Neuron Disord 1:163–184
18. Kato S, Nakashima K, Horiuchi S, Nagai R, Cleveland DW, Liu J, Hirano A, Takikawa M, Kato M, Nakano I, Sakoda S, Asayama K, Ohama E (2001) Formation of advanced glycation end-product-modified superoxide dismutase-1 (SOD1) is one of the mechanisms responsible for inclusions common to familial amyotrophic lateral sclerosis patients with SOD1 gene mutation, and transgenic mice expressing human SOD1 gene mutation. Neuropathology 21:67–81
19. Kato S, Sumi-Akamaru H, Fujimura H, Sakoda S, Kato M, Hirano A, Takikawa M, Ohama E (2001) Copper chaperone for superoxide dismutase co-aggregates with superoxide dismutase 1 (SOD1) in neuronal Lewy body-like hyaline inclusions: an immunohistochemical study on familial amyotrophic lateral sclerosis with SOD1 gene mutation. Acta Neuropathol 102:233–238
20. Kato T, Hirano A, Kurland LT (1987) Asymmetric involvement of the spinal cord involving both large and small anterior horn cells in a case of familial amyotrophic lateral sclerosis. Clin Neuropathol 6:67–70
21. Kosower NS, Kosower EM (1978) The glutathione status of cells. Int Rev Cytol 54:109–160
22. Kurland LT, Mulder DW (1955) Epidemiologic investigations of amyotrophic lateral sclerosis. II. Familial aggregations indicative of dominant inheritance. Neurology 5:249–268
23. Matsumoto A, Okado A, Fujii T, Fujii J, Egashira M, Niikawa N, Taniguchi N (1999) Cloning of the peroxiredoxin gene family in rats and characterization of the fourth member. FEBS Lett 443:246–250
24. Meister A, Anderson ME (1983) Glutathione. Annu Rev Biochem 52:711–760
25. Mills GC (1957) Hemoglobin catabolism. 1. Glutathione peroxidase, an erythrocyte enzyme which protects hemoglobin from oxidative breakdown. J Biol Chem 229:189–197
26. Mu ZM, Yin XY, Prochownik EV (2002) Pag, a putative tumor suppressor, interacts with the Myc Box II domain of c-Myc and selectively alters its biological function and target gene expression. J Biol Chem 277:43175–43184

27. Nagai M, Aoki M, Miyoshi I, Kato M, Pasinelli P, Kasai N, Brown RH Jr, Itoyama Y (2001) Rats expressing human cytosolic copper-zinc superoxide dismutase transgenes with amyotrophic lateral sclerosis: associated mutations develop motor neuron disease. J Neurosci 21:9246–9254
28. Nakano I, Hirano A, Kurland LT, Mulder DW, Holley PW, Saccomanno G (1984) Familial amyotrophic lateral sclerosis. Neuropathology of two brothers in American "C" family. Neurol Med (Tokyo) 20:458–471
29. Sen CK, Packer L (1996) Antioxidant and redox regulation of gene transcription. FASEB J 10:709–720
30. Shibata N, Hirano A, Kobayashi M, Siddique T, Deng HX, Hung WY, Kato T, Asayama K (1996) Intense superoxide dismutase-1 immunoreactivity in intracytoplasmic hyaline inclusions of familial amyotrophic lateral sclerosis with posterior column involvement. J Neuropathol Exp Neurol 55:481–490
31. Takahashi K, Nakamura H, Okada E (1972) Hereditary amyotrophic lateral sclerosis. Histochemical and electron microscopic study of hyaline inclusions in motor neurons. Arch Neurol 27:292–299
32. Watanabe M, Dykes-Hoberg M, Culotta VC, Price DL, Wong PC, Rothstein JD (2001) Histological evidence of protein aggregation in mutant SOD1 transgenic mice and in amyotrophic lateral sclerosis neural tissues. Neurobiol Dis 8:933–941
33. Wen ST, Van Etten RA (1997) The PAG gene product, a stress-induced protein with antioxidant properties, is an Abl SH3-binding protein and a physiological inhibitor of c-Abl tyrosine kinase activity. Genes Dev 11:2456–2467

J_ID: Z3P Customer A_ID: H043 Cadmus Art: JNR2780 Date: 22-FEBRUARY-05 Stage: I

Journal of Neuroscience Research 80:000–000 (2005)

Transplantation of Human Neural Stem Cells for Spinal Cord Injury in Primates

A. Iwanami,[1–3] S. Kaneko,[1–3] M. Nakamura,[2*] Y. Kanemura,[4,5] H. Mori,[4] S. Kobayashi,[4] M. Yamasaki,[5,6] S. Momoshima,[7] H. Ishii,[8] K. Ando,[8] Y. Tanioka,[8] N. Tamaoki,[8] T. Nomura,[8] Y. Toyama,[2] and H. Okano[1,3]

[1]Department of Physiology, Keio University School of Medicine, Shinjuku, Tokyo, Japan
[2]Department of Orthopaedic Surgery, Keio University School of Medicine, Shinjuku, Tokyo, Japan
[3]Core Research for Evolutional Science and Technology (CREST), Japan Science and Technology Agency (JST), Kawaguchi, Saitama, Japan
[4]Tissue Engineering Research Center (TERC), National Institute of Advanced Industrial Science and Technology (AIST), Amagasaki, Hyogo, Japan
[5]Institute for Clinical Research, Osaka National Hospital, Osaka, Japan
[6]Department of Neurosurgery, Osaka National Hospital, Osaka, Japan
[7]Department of Radiology, Keio University School of Medicine, Shinjuku, Tokyo, Japan
[8]Central Institute for Experimental Animals, Kawasaki, Kanagawa, Japan

Recent studies have shown that delayed transplantation of neural stem/progenitor cells (NSPCs) into the injured spinal cord can promote functional recovery in adult rats. Preclinical studies using nonhuman primates, however, are necessary before NSPCs can be used in clinical trials to treat human patients with spinal cord injury (SCI). Cervical contusion SCIs were induced in 10 adult common marmosets using a stereotaxic device. Nine days after injury, in vitro-expanded human NSPCs were transplanted into the spinal cord of five randomly selected animals, and the other sham-operated control animals received culture medium alone. Motor functions were evaluated through measurements of bar grip power and spontaneous motor activity, and temporal changes in the intramedullary signals were monitored by magnetic resonance imaging. Eight weeks after transplantation, all animals were sacrificed. Histologic analysis revealed that the grafted human NSPCs survived and differentiated into neurons, astrocytes, and oligodendrocytes, and that the cavities were smaller than were those in sham-operated control animals. The bar grip power and the spontaneous motor activity of the transplanted animals was significantly higher than that of sham-operated control animals. These findings show that NSPC transplantation was effective for SCI in primates and suggest that human NSPC transplantation could be a feasible treatment for human SCI.

Key words: spinal cord injury; transplantation; neural stem/progenitor cells; primate; preclinical study

Recovery from damage to the adult mammalian central nervous system (CNS), especially spinal cord injury (SCI), is hindered by various factors (Horner and Gage, 2000; Okano, 2002), such as the limited ability of the CNS to replace lost cells (Johansson et al., 1999), axonal growth inhibitors associated with myelin and glial scars (Olson, 2002; David and Lacroix, 2003), and insufficient trophic support (Widenfalk et al., 2001). With the recent progress in stem cell biology, embryonic stem (ES) cell-derived cells (McDonald et al., 1999), mesenchymal stem cells (Hofstetter et al., 2002), olfactory ensheathing cells (Li et al., 1997), and neural stem/progenitor cells (NSPCs) (Cao et al., 2001; Ogawa et al., 2002) have become hopeful candidates for transplantation to treat SCI. Recently, we demonstrated that the timing of NSPC transplantation is crucial for the survival and differentiation of grafted cells and functional recovery in terms of the microenvironment of the injured spinal cord (Ogawa et al., 2002; Okano, 2002; Nakamura et al., 2003; Okano et al., 2003). Based on these findings, we transplanted NSPCs into the adult rat spinal cord 9 days after injury and demonstrated the usefulness of in vitro-expanded NSPCs as a therapeutic tool for the treatment of SCI (Ogawa et al., 2002). Despite these promising results, the rat model is not an ideal preclinical model for human SCI because neurofunctional and ana-

A. Iwanami and S. Kaneko contributed equally to this work.

Contract grant sponsor: Japanese Ministry of Education, Sports and Culture; Contract grant sponsor: Human Frontier Science Program Organization; Contract grant sponsor: Core Research for Evolutional Science and Technology (CREST), Japan Science and Technology Corporation (JST); Contract grant sponsor: General Insurance Association of Japan; Contract grant sponsor: Keio University. AQ1

*Correspondence to: Masaya Nakamura, Department of Orthopaedic Surgery, Keio University School of Medicine, 35 Shinanomachi, Shinjuku, Tokyo, 160-8582, Japan. E-mail: masa@sc.itc.keio.ac.jp AQ2

Received 30 November 2004; Revised 4 January 2005; Accepted 5 January 2005

Published online 00 Month 2005 in Wiley InterScience (www.interscience.wiley.com). DOI: 10.1002/jnr.20436

J_ID: Z3P Customer A_ID: H043 Cadmus Art: JNR2780 Date: 22-FEBRUARY-05 Stage: I

tomic features of rodents and primates are different. For example, the corticospinal tract (CST) fibers localize mainly in the dorsal funiculus in rodents whereas in primates, they localize mainly in the lateral funiculus (Terashima et al., 1994; Iwanami et al., 2005). Recently, hemisection SCI models in primates have been reported (Levi et al., 2002; Tuszynski et al., 2002). A hemisection model is appropriate for demonstrating regeneration of axons, but from a clinical point of view, it is not suitable as a model of human SCI because human SCI is mainly a contusion injury that occurs when the spine is subjected to an external force through accidents or falls from a height. We therefore established a graded-contusive SCI model in common marmosets (*Callithrix jacchus*), which were quite similar to the characteristics of human SCI (Iwanami et al., 2005), and examined the effectiveness of human NSPC transplantation on recovery of motor functions in tetraplegic primates after contusive SCI.

MATERIALS AND METHODS

Tissue Samples, Neurosphere Cultures, and Differentiation Assays

The ethical committees of Osaka National Hospital, the Tissue Engineering Research Center, and Keio University approved the use of human fetal neural tissues and neurosphere cultures. Tissue procurement procedures were in accordance with the Declaration of Helsinki and in agreement with the ethical guidelines of the Japan Society of Obstetrics and Gynecology. Human fetuses (8 weeks gestational age) were obtained from legal abortions carried out at the Osaka National Hospital with written informed consent obtained from all donors. NSPCs were cultured from fetal spinal cord tissue using the neurosphere method (Svendsen et al., 1998; Kanemura et al., 2002), and differentiation assays were carried out as described previously (Kanemura et al., 2002).

Contusive SCIs and Transplantation of Human NSPCs in Marmosets

Ten adult female common marmosets (280–350 g; Clea Japan Inc., Tokyo, Japan) were used for these experiments. Contusive SCIs were induced using a weight-drop device (a modified NYU impactor with a diameter of 3.5 mm) to establish an SCI model (Gruner, 1992). After an intramuscular injection of ketamine (50 mg/kg) and xylazine (5 mg/kg) to induce anesthesia, a C5 laminectomy was carried out and a 17-g weight was dropped from a height of 50 mm onto the exposed dura matter (moderate injury; Iwanami et al., 2005). Human NSPCs that had undergone more than 10 passages were selected and transplanted into the injured spinal cord 9 days after the injury, at which time the microenvironment of the injured spinal cord changes from that of the inhospitable acute phase to one that supports the survival and differentiation of transplanted NSPCs (Ogawa et al., 2002; Okano, 2002; Nakamura et al., 2003; Okano et al., 2003). The neurospheres were prelabeled with 5-bromo-2′-deoxyuridine (BrdU) in vitro (3 μM, Sigma-Aldrich Corp., St. Louis, MO) for 72 hr before transplantation. Nine days after the injury, partially dissociated neurospheres (dissociated to a diameter of <100 μm so they could pass through the microglass pipette used in transplantation) at a density of approximately 1.0×10^6 cells/5 μl of medium without growth factors (TP; $n = 5$) or 5 μl of the medium vehicle without growth factors (CON; $n = 5$) were injected into the center of the lesion site using a glass pipette (diameter of the tip = 100 μm) configured to a 10-μl Hamilton syringe and a microstereotaxic injection system (David Kopf Instruments, Tujunga, CA). All animals received daily ampicillin (100 mg/kg intramuscularly; Meiji Seika Kaisha, Ltd., Tokyo, Japan) for 1 week after injury and daily cyclosporine injections (10 mg/kg subcutaneously; Novartis, Basel, Switzerland) for 8 weeks after transplantation. The ethics committee of the institute approved all surgical interventions and animal care procedures, which were in accordance with the Laboratory Animal Welfare Act, the Guide for the Care and Use of Laboratory Animals (National Institutes of Health, USA), and the Guidelines and Policies for Animal Surgery provided by the Animal Study Committees of the Central Institute for Experimental Animals and Keio University.

Magnetic Resonance Imaging Evaluation

The magnitude of the SCI was monitored by examining changes in intramedullary magnetic resonance imaging (MRI) signals, because pathogenic events, such as hemorrhage, edema, and cavity formation can be monitored in real time using MRI techniques (Ohta et al., 1999; Metz et al., 2000). Images were obtained using a 1.5-Tesla superconducting imager (Signa, Milwaukee, WI) with a phased-array volume coil under the following conditions: (1) sagittal; and (2) axial T2-weighted fast spin-echo with a repetition/echo time (TR/TE) number averaging 4,000 msec/100 msec/15, a field-of-view of 9 cm, a matrix of 256 × 256, and a section thickness of 1.7 mm; and (3) sagittal T1-weighted spin-echo with a TR/TE number averaging 400 msec/12 msec/15 and all other parameters the same as above.

Behavioral Testing

Motor functions were assessed using the bar grip test and the monitoring of spontaneous movements (see Iwanami et al., 2005). In brief, to examine the neuromuscular function of both forelimbs, the peak grasping strength of both forelimbs was evaluated three times a day before and after transplantation using a specially designed pull-bar assembly with a gauge (A&D, Tokyo, Japan; Smith et al., 1995; Suresh Babu et al., 2000). The spontaneous three-dimensional (3D) movement of each marmoset was monitored using an infrared sensor (Neuroscience, Tokyo, Japan) placed in the ceiling of each cage, and an hourly activity count was recorded. The grip power and motor activity of the TP and CON groups were then compared statistically using the Mann-Whitney *U*-test.

Histologic Analyses

Eight weeks after transplantation, each animal was intracardially perfused with 4% paraformaldehyde (PFA; pH 7.4). The dissected spinal cord tissues were postfixed for 3 hr in 4% PFA, soaked overnight in 10% followed by 30% sucrose, and

J_ID: Z3P Customer A_ID: H043 Cadmus Art: JNR2780 Date: 22-FEBRUARY-05 Stage: I

cut into 20-μm thick axial sections using a cryostat. Hematoxylin-eosin (HE) staining was carried out for general histologic examinations. The myelinated area was stained with Luxol fast blue (LFB) and the myelinated area at the lesion epicenter of five randomly selected axial sections was quantified by a Micro-Computer Imaging Device (MCID; Amersham Biosciences Corp., Piscataway, NJ). To quantify the number of motor neurons, axial sections (every 10th section within 1.5 mm of the lesion epicenter and every 50th section in areas more than 1.5 mm distant from the lesion epicenter) were immunostained with anti-choline acetyltransferase (ChAT) antibody (1:25 mouse IgG; Chemicon International, Inc., Temecula, CA) and the number of ChAT-positive cells located in the ventral horn of each section was counted. The myelinated area and the numbers of ChAT-positive cells of the TP and CON groups were then statistically compared using the Mann-Whitney *U*-test.

To examine the distribution of NSPCs grafted into the injured spinal cords, sections were immunostained using an anti-BrdU antibody (mouse IgG, BrdU staining kit; Zymed Lab. Inc., South San Francisco, CA) visualized with diaminobenzidine (DAB) solution. The phenotype of the grafted cells were assessed through fluorescent double immunostaining using an anti-BrdU antibody and one of the following cell-type specific markers: anti-β-tubulin III antibody (1:400, mouse IgG; BAbCO, Berkley, CA), anti-glial fibrillary acidic protein (GFAP) antibody (1:200, rabbit IgG; Dako Japan, Tokyo, Japan), anti-Olig2 antibody (1:400; a kind gift of M. Nakafuku, Cincinnati Children's Hospital Research Foundation; Zhou et al., 2001; Mizuguchi et al., 2001), or anti-CNPase antibody (1:500, mouse IgG; Sigma-Aldrich). To evaluate the correlation between grafted cells and axons around the lesion epicenter, double immunostaining visualized with Vectastain ABC system (Vector Laboratories, Inc., Burlingame, CA) or fluorescent double immunostaining using anti-BrdU and anti-neurofilament 200 kDa (RT-97) antibodies (1:1,000, mouse IgG; Chemicon International) were carried out. The secondary antibodies were as follows: Alexa Fluor 488 goat anti-mouse IgG; 568 goat anti-mouse IgG; and 568 goat anti-rabbit IgG (1:1,000; Molecular Probes, Eugene, OR). Grafted NSPCs that were colabeled with both BrdU and cell-specific markers were observed under a confocal microscope equipped with an argon-krypton laser (LSM510; Carl Zeiss Co., Ltd., Oberkochen, Germany), at a magnification of 400×. The number of BrdU-positive cells, double-positive cells for BrdU, and each marker at the lesion epicenter in five randomly captured images of 10 sections were counted and the proportion of double-positive cells to BrdU-positive cells was calculated.

RESULTS

MRI and Histology of Injured Spinal Cord after NSPC Transplantation

Five days after injury, an iso-signal intensity area on T1-weighted images (T1WI) and a homogeneously high signal intensity area on T2-weighted images (T2WI) indicating the presence of hemorrhage as well as edema were observed at the epicenter of the lesion (Fig. 1A). Eight weeks after the transplantation, the lesion site appeared as a clearly demarcated low signal intensity area on T1WI and a high signal intensity area on T2WI in both the TP and CON groups, but the size of the lesion was visibly smaller in the TP group (Fig. 1B,C). Subsequent histologic analyses revealed that the intramedullary signal changes observed on MRI corresponded to the formation of a cavity accompanied by reactive gliosis, void of β-tubulin III-positive neurons (Fig. 1D–F). The cavity at the epicenter of the injury site was smaller in the TP animals (Fig. 1D,F), consistent with the MRI findings (Fig. 1B,C). In contrast, quantitative analysis of the myelinated area and number of ChAT-positive neurons at the lesion epicenter revealed no significant differences between the two groups (data not shown). To elucidate the mechanism through which NSPC transplantation reduces the size of cavity, the phenotypes of human NSPC-derived cells both before and after transplantation were examined.

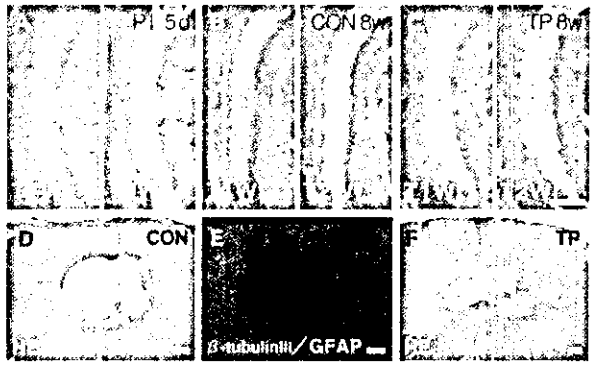

COLOR

Fig. 1. Comparison of MR images and histology between CON and TP groups. **A–C:** Sagittal MR image; T1WI (left), T2WI (right). Post-injury intramedullary signal changes in marmosets were similar to those seen in humans. Scale bar = 2.5 mm. **D, F:** Hematoxylin-eosin staining (axial section). The signal changes seen on MRI coincide with the formation of a cavity at the site of the injury. **E:** GFAP (green)/β-tubulin III (red) double-labeled image; axial section. Scale bar = 50 μm. Reactive gliosis surrounding the cavities, void of neurons. A: Five days post-injury. B, D, E: Results from a typical CON animal 8 weeks after transplantation. C, F: Results from a typical TP animal 8 weeks after transplantation.

Phenotypes of Human NSPCs Before and After Differentiation in Vitro

The phenotypes of human NSPCs before and after differentiation in vitro were examined after labeling the cells with BrdU (Kanemura et al., 2002). Before differentiation was induced, the neurospheres of human NSPCs consisted of a heterogenous mix of cells such as nestin-positive cells, β-tubulin III-positive cells, and GFAP-positive cells (Fig. 2A–L). Quantitative analyses revealed that the BrdU-positive NSPCs consisted of 51.9 ± 2.7% nestin-positive cells, 12.8 ± 1.8% β-tubulin III-positive cells, and 34.5 ± 4.2% GFAP-positive cells (Table I). Seven days after differentiation was induced, nestin-positive cells became undetectable,

J_ID: Z3P Customer A_ID: H043 Cadmus Art: JNR2780 Date: 22-FEBRUARY-05 Stage: I

COLOR

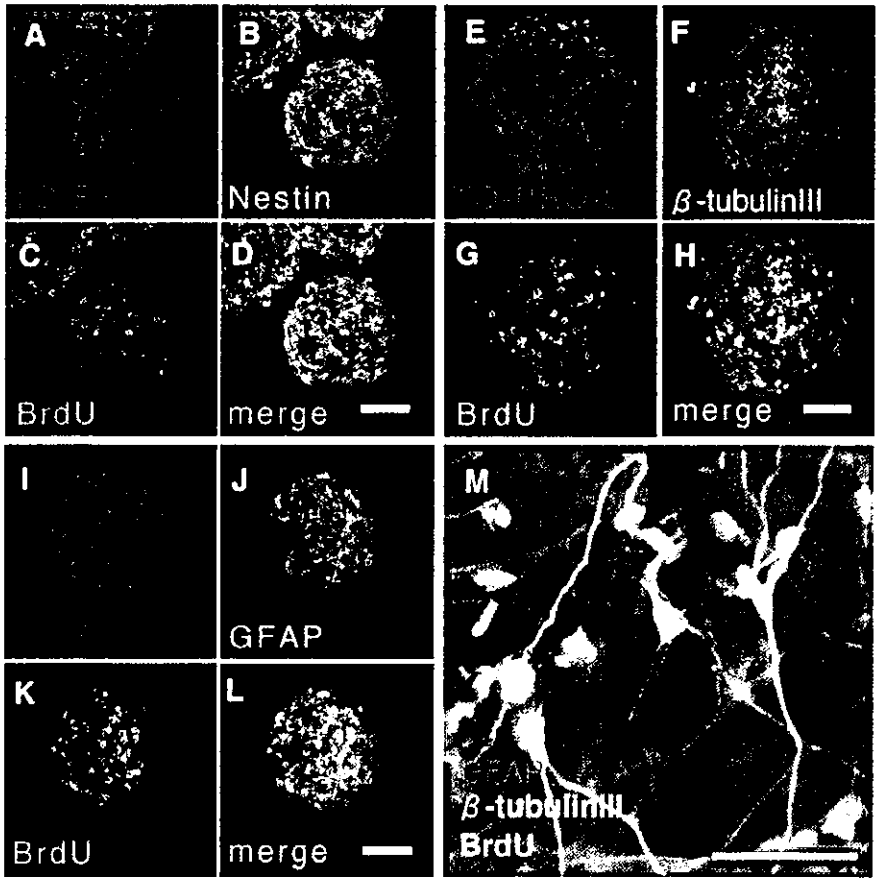

Fig. 2. Typical image of human NSPCs before and after differentiation in vitro. Immunofluorescence analysis of in vitro human NSPCs before (A–L) and after (M) differentiation stained with selective phenotypic markers. A, E, I: TO-PRO-3 (Molecular Probes), blue, was used to label nuclei. B: Anti-human nestin (red). F: β-Tubulin III (red). J: GFAP (red). C, G, K: BrdU (green). The three images shown in each panel were merged in D, H, and L. M: Typical image of human NSPCs after differentiation triple-stained with BrdU (green), β-tubulin III (red), and GFAP (blue). Photomicrographs of human NSPCs after differentiation in vitro immunostained with selective phenotypic markers: triple-stained with BrdU (green), β-tubulin III (red), and GFAP (blue). Scale bars = 50 μm.

AQ6

GFAP-positive cells increased to 85.6 ± 1.6%, and the percentage of β-tubulin III-positive cells was unchanged (11.4 ± 0.3%) (Fig 2M). Olig2-positive cells, indicating progenitor cells of oligodendrocyte lineages or motor neurons (Mizuguchi et al., 2001; Zhou et al., 2001), were not observed before or after differentiation in vitro (Table I). These results suggested that most nestin-positive cells differentiated into astrocytes in vitro.

Grafted Human NSPCs Survived and Differentiated Into Neuronal and Glial Lineages

To examine the fate of NSPCs grafted into the injured spinal cord, fluorescent double immunostaining for BrdU and cell-specific markers, such as β-tubulin III, GFAP, or Olig2 was carried out. In the TP group, BrdU-positive cells were detected mainly around the grafted sites (Fig. 3A), but some were distributed as far as 8 mm rostral and caudal to the epicenter 8 weeks after transplantation. No evidence of tumor formation was observed in the TP group. Quantitative analysis using confocal microscopy revealed that 20.6 ± 1.9% of the BrdU-positive cells were β-tubulin III-positive, 46.2 ± 2.1% were GFAP-positive, and 5.3 ± 0.9% were Olig2-positive (Fig. 3B–D; Table I). β-Tubulin III/Olig2/BrdU triple-positive cells were not identified, indicating that the Olig2-positive cells were not progenitors for motor neurons or other neurons; however, CNPase/BrdU double-positive cells were detected around the grafted site (data not shown). In contrast, 25.2 ± 2.9% of the BrdU-positive cells were nestin positive, suggesting that part of the grafted NSPCs remained immature within the host spinal cord after the transplantation. A bundle of RT-97 positive fibers were observed at the lesion epicenter in the TP group (Fig. 3E), but not in the CON group. These fibers were associated closely with the grafted human NSPCs (Fig. 3F,G).

F3

Human NSPC Transplantation Promoted Functional Recovery After SCI in Primates

All animals were tetraplegic immediately after awakening from anesthesia. For a few days after surgery the animals could hardly move around, but they began to gradually recover thereafter. Recovery of motor function was observed mainly in the hindlimbs, with paralytic symptoms clearly persisting in the forelimbs. To evaluate the recovery of forelimb motor function, daily bar grip tests were conducted. The mean value of 10 animals' bar grip power sharply decreased from 30.9 ±

J_ID: Z3P Customer A_ID: H043 Cadmus Art: JNR2780 Date: 22-FEBRUARY-05 Stage: I

TABLE I. Percentage of Cell Types Derived From Human Neural Stem/Progenitor Cells In Vitro and In Vivo*

Condition	Cell type (%)			
	Nestin	β-tubulin III	GFAP	Olig2
Before differentiation in vitro	51.9 ± 2.7	12.8 ± 1.8	34.5 ± 4.2	0
After differentiation in vitro	0	11.4 ± 0.3	85.6 ± 1.6	0
After transplantation in vivo	25.2 ± 2.9	20.6 ± 1.9	46.2 ± 2.1	5.3 ± 0.9

*The percentages (mean ± standard deviation) of differentiated cell types derived from the donor cells in vivo were different from those in vitro. The percentage of β-tubulin III/BrdU double-positive cells among the BrdU-positive cells in vivo was almost twice the percentage in vitro, and Olig2/BrdU double-positive cells were detected only in vivo. GFAP, glial fibrillary acidic protein. AQ7,8

2.3 to 5.4 ± 1.4 N after injury, followed by a partial recovery (9.7 ± 1.6 N) at 7 days after the injury. No significant differences in the mean value of bar grip power between the TP and CON groups were observed at any time point before the transplantation. After transplantation the TP animals showed improved recovery, with significantly higher bar grip power values than the CON animals at 2–4 weeks and 7–8 weeks after transplantation (Fig. 4A). F4

After SCI, the number of spontaneous movements in both the TP and CON groups decreased sharply (9.2 ± 2.2% of the preinjury level), followed by a partial recovery (32.4 ± 8.7%) at the time of transplantation. No significant differences in the mean value of the number of spontaneous movements were observed between the TP and CON groups at any time point before transplantation. After transplantation the TP animals showed improved recovery, with significantly higher spontaneous movement values than CON animals at 1, 3, and 8 weeks after transplantation (Fig. 4B).

DISCUSSION

Results of the present study suggest that transplantation of human NSPCs into the contused spinal cord of common marmosets at 9 days after injury survived, differentiated into neurons, astrocytes, and oligodendrocytes and promoted functional recovery. These findings suggest the clinical significance of human NSPC transplantation to injured spinal cords in primates.

Compared to other kinds of primates such as macaques and bonnet monkeys, common marmosets offer several advantages to scientific studies: small body size, adaptability to a variety of conditions, and a high rate of breeding. Common marmosets have become quite popular among researchers, being incorporated into numerous preclinical models ('t Hart et al., 2000; Kirik et al., 2003; Mansfield et al., 2003), but reports of SCI in primates are limited (Emery et al., 2000; Liu et al., 2001). In our models of contusive SCI in marmosets, approximately 85% of cholinergic neurons and 80% of myelination were lost and MRI depicted the formation of a cystic cavity accompanied by glial scarring at the lesion epicenter (Iwanami et al., 2005). This model of contusive SCI in common marmosets reproduces the symptoms seen in incomplete cervical SCI in humans, and is an ideal model for preclinical trials of various SCI therapies. AQ3

Histologic and MRI findings revealed that the transplantation of human NSPCs reduced the size of the cavity, but this occurred without a significant reduction in the demyelinated area or an increase in the numbers of ChAT-positive neurons at the lesion site. Postulating that the survival of the grafted cells played a part in reducing the size of the cavity, the phenotype of human NSPCs were examined not only in vivo, but also in vitro. Intriguingly, the percentages of differentiated cell types derived from donor cells in vivo were quite different from those in vitro: the percentage of β-tubulin III-positive cells in vivo was almost twice as much as that in vitro, and Olig2-positive cells were detected in vivo but not in vitro (Table I). These results suggested that the microenvironment within the spinal cord at 9 days after the injury induced differentiation of grafted human NSPCs into cells of neuronal and oligodendrocyte lineages, similar to the findings in the rat SCI model (Ogawa et al., 2002; Okano, 2002; Okano et al., 2003). Approximately 46% and 25% of the grafted NSPCs were GFAP-positive cells and nestin-positive immature cells, respectively. These astrocytes and undifferentiated cells as well as neurons derived from grafted NSPCs might have reduced the size of the cavity at the lesion site. Neurons derived from NSPCs were observed in this study in contrast to the report by Cao et al. (2001) in which subventricular zone-derived NSPCs grafted into the intact or injured spinal cord of adult rats 10 days after injury survived, migrated, and differentiated into astrocytes and oligodendrocytes, but not into neurons. The difference in cell preparation and transplantation methods may have resulted in the contrasting results. As we reported previously (Watanabe et al., 2004), the NSPCs derived from the forebrain were able to differentiate into neurons in the injured rat spinal cord when transplanted 9 days after injury. This might be partly because neurospheres and not single cells were transplanted in our studies, because cell–cell contacts as well as autocrine and paracrine factors within the neurospheres play an important role in their survival and neuronal differentiation (Taupin et al., 2000). Another recent study suggested that NSPCs differentiated into

J_ID: Z3P Customer A_ID: H043 Cadmus Art: JNR2780 Date: 22-FEBRUARY-05 Stage: I

COLOR

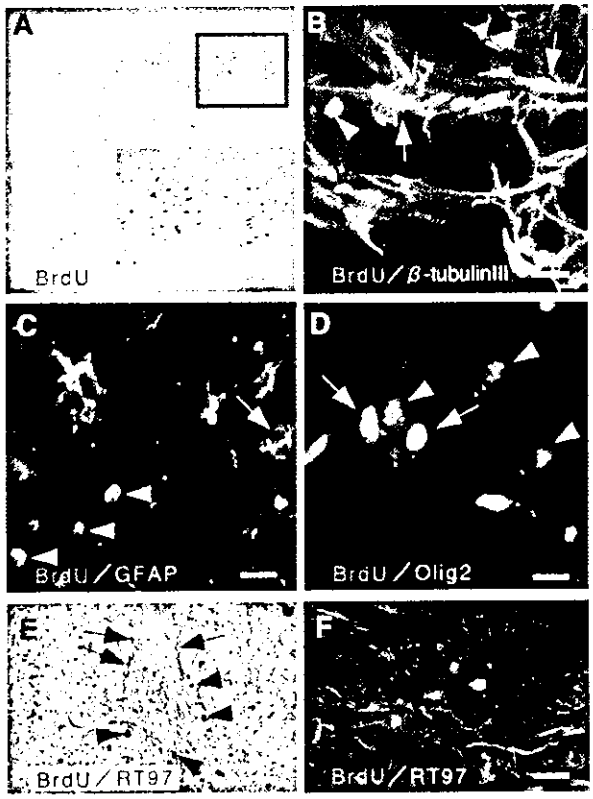

Fig. 3. Grafted human NSPCs survived and differentiated into neurons, astrocytes, and oligodendrocytes within injured marmoset spinal cord. **A:** BrdU immunostaining of an axial section (DAB) in a TP animal. **B–D, G:** Confocal images reveal double labeling for anti-BrdU (green) and anti-β-tubulin III (red) in B, anti-GFAP (red) in C, anti-Olig2 (red) in D, and anti-RT-97 (red) in F. Arrows, double-positive cells of BrdU and each marker in B–D; arrowheads, BrdU-positive NSPCs that are negative for each marker in B–D. **E, F:** Grafted NSPCs were associated closely with RT-97-positive fibers at the lesion epicenter. E: Arrowheads (dark brown), BrdU-positive NSPCs; arrows (light brown), RT-97-positive fibers. Sections were counterstained with hematoxylin to identify nuclei. F: BrdU (green), RT-97 (red). Scale bars = 25 μm (A); 50 μm (B–F).

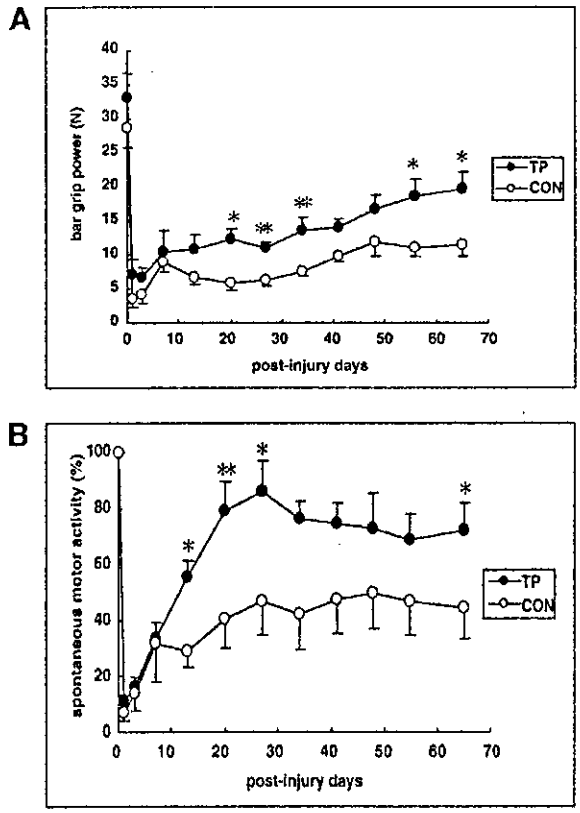

Fig. 4. Behavioral testing and promotion of functional recovery by grafted human NSPCs after SCI. **A:** Time-course of the bar grip power in the TP group (filled circles) and CON group (open circles); $n = 5$ per group. $^{*}P < 0.05$; $^{**}P < 0.01$ compared to the CON group at the same time point (Mann-Whitney *U*-test). The bar grip power of the TP animals improved significantly compared to that of the CON animals at 2–4 weeks and 7–8 weeks after transplantation. **B:** Time-course of the spontaneous motor activity in the TP (filled circles) and CON (open circles) groups; $n = 5$ per group. $^{*}P < 0.05$; $^{**}P < 0.01$. The mean values of spontaneous movements of TP animals were significantly higher than were that of the CON animals at 1, 3, and 8 weeks after transplantation. Data represent the mean ± standard error of the mean.

glial lineage when transplanted immediately after SCI (Vroemen et al., 2003). The microenvironment within the injured spinal cord at 9 days after injury might also be advantageous for survival and neuronal differentiation of the grafted NSPCs compared to that in the acute inflammatory phase (Miyoshi et al., 1995; Okano, 2002; Nakamura et al., 2003; Okano et al., 2003; Okada et al., 2004).

Without human NSPC transplantation, contusive SCI in common marmosets resulted in an approximately 65% loss of grip power of the forelimbs and a 60% loss of spontaneous motor activity. In contrast, transplantation of human NSPCs significantly promoted functional recovery. Three possible explanations for this improvement may be made, based on our findings and the findings of previous studies using rodents (Horner and Gage, 2000; Okano, 2002; Schwab, 2002; Okano et al., 2003). One possibility is that immature astrocytes derived from grafted NSPCs might play an important role in axonal guidance (Hofstetter et al., 2002; Silver and Miller, 2004). In the present study, astrocytes accounted for most cells that differentiated from the human fetal CNS-derived NSPCs. These astrocytes might have played active roles in generation of neuronal cells and axonal regeneration of host neuronal axons. Notably, fetal brain-derived astrocytes have been shown to regulate the precise growth of neuronal axons (Garcia-Abreu et al., 2000) and to promote the physiologic maturation of

J_ID: Z3P Customer A_ID: H043 Cadmus Art: JNR2780 Date: 22-FEBRUARY-05 Stage: I

neuronal cells (Blondel et al., 2000). The second possible explanation is that the neurons differentiated from NSPCs formed new synapses with the host neurons aiding to reform the neuronal circuits that had been disrupted by the injury (Ogawa et al., 2002; Okano et al., 2003). Synapse formation by donor-derived inhibitory neurons might also be important for motor coordination within the spinal neuronal network as well as for the suppression of injury-induced spasticity (Campos et al., 2004; Watanabe et al., 2004). The third possibility is that trophic effects (indicating that functional improvement may not be dependent on the transplanted human NSPCs becoming functional neurons and making the right connections, but rather on the secretion of trophic factors from the transplanted cells) might also be effective for the survival and differentiation of host cells in the injured spinal cord, leading to functional recovery (Namiki et al., 2000; Koda et al., 2002). The molecular nature of these trophic factors should be identified in the future studies.

In conclusion, the transplantation of in vitro-expanded human NSPCs into the injured spinal cord 9 days after contusion injury resulted in the survival of the transplanted cells for at least 8 weeks, differentiation of the transplanted cells into neurons, astrocytes, and oligodendrocytes, and improved motor functional recovery without the formation of tumors. To treat SCI patients effectively using NSPC transplantation, additional strategies to promote regeneration of injured axons will be required, such as the concomitant use of scaffolds (Teng et al., 2002), the blockage of axonal regeneration inhibitors (Domeniconi et al., 2002; GrandPre et al., 2002), and the administration of neurotrophic factors (Grill et al., 1997; Liu et al., 1999). The differences in anatomy and functional neuronal circuits of the spinal cord between rodents and primates make the primate SCI model a powerful tool in the preclinical evaluation of prospective cell transplantation therapy protocols for human SCI. The transplantation of human NSPCs into the contused marmoset spinal cord may act as a bridge between rodent and human trials.

ACKNOWLEDGMENTS

This work was supported by a project to realize regenerative medicine from the Japanese Ministry of Education, Sports and Culture, the Human Frontier Science Program Organization, Core Research for Evolutional Science and Technology (CREST) from the Japan Science and Technology Corporation (JST), the General Insurance Association of Japan, a National Grant-in-Aid for the Establishment of a High-Tech Research Center in a Private University in Japan, a Keio University special grant-in-aid for innovative collaborative research projects (to H.O.), a grant-in-aid from the 21st Century COE Program of the Ministry of Education, Culture, Sports, Science and Technology, Japan to Keio University, and a Keio University grant-in-aid for the encouragement of young medical scientists (to A.I.).

We thank Mrs. A. Hirayama for her arrangement of the figures and to all the other members of the Okano Laboratory for their enthusiastic discussions, encouragement, and invaluable comments on this article. AQ1

REFERENCES

Blondel O, Collin C, McCarran WJ, Zhu S, Zamostiano R, Gozes I, Brenneman DE, McKay RD. 2000. A glial-derived signal regulating neuronal differentiation. J Neurosci 20:8012–8020.

Campos L, Meng Z, Hu G, Chiu DT, Ambron RT, Martin JH. 2004. Engineering novel spinal circuits to promote recovery after spinal injury. J Neurosci 24:2090–2101.

Cao QL, Zhang YP, Howard RM, Walters WM, Tsoulfas P, Whittemore SR. 2001. Pluripotent stem cells engrafted into the normal or lesioned adult rat spinal cord are restricted to a glial lineage. Exp Neurol 167:48–58.

David S, Lacroix S. 2003. Molecular approaches to spinal cord repair. Annu Rev Neurosci 26:411–440.

Domeniconi M, Cao Z, Spencer T, Sivasankaran R, Wang K, Nikulina E, Kimura N, Cai H, Deng K, Gao Y, He Z, Filbin M. 2002. Myelin-associated glycoprotein interacts with the Nogo66 receptor to inhibit neurite outgrowth. Neuron 35:283–290.

Emery E, Rhrich-Haddout F, Kassar-Duchossoy L, Lyoussi B, Tadie M, Horvat JC. 2000. Motoneurons of the adult marmoset can grow axons and reform motor endplates through a peripheral nerve bridge joining the locally injured cervical spinal cord to the denervated biceps barachii muscle. J Neurosci Res 62:821–829.

Garcia-Abreu J, Mendes FA, Onofre GR, De Freitas MS, Silva LC, Moura Neto V, Cavalcante LA. 2000. Contribution of heparan sulfate to the nonpermissive role of the midline glia to the growth of midbrain neurites. Glia 29:260–272.

GrandPre T, Li S, Strittmatter SM. 2002. Nogo-66 receptor antagonist peptide promotes axonal regeneration. Nature 417:547–551.

Grill R, Murai K, Blesch A, Gage FH, Tuszynski MH. 1997. Cellular delivery of neurotrophin-3 promotes corticospinal axonal growth and partial functional recovery after spinal cord injury. J Neurosci 17:5560–5572.

Gruner JA. 1992. A monitored contusion model of spinal cord injury in the rat. J Neurotrauma 9:123–128.

Hofstetter CP, Schwarz EJ, Hess D, Widenfalk J, El Manira A, Prockop DJ, Olson L. 2002. Marrow stromal cells form guiding strands in the injured spinal cord and promote recovery. Proc Natl Acad Sci USA 99:2199–2204.

Horner PJ, Gage FH. 2000. Regenerating the damaged central nervous system. Nature 407:963–970.

Iwanami A, Yamane J, Katoh H, Nakamura M, Momoshima S, Ishii H, Tanioka Y, Tamaoki N, Nomura T, Toyama Y, Okano H. 2005. Establishment of graded spinal cord injury model in a nonhuman primate: the common marmoset. J Neurosci Res (this issue). AQ3

Johansson CB, Momma S, Clarke DL, Risling M, Lendahl U, Frisen J. 1999. Identification of a neural stem cell in the adult mammalian central nervous system. Cell 96:25–34.

Kanemura Y, Mori H, Kobayashi S, Islam O, Kodama E, Yamamoto A, Nakanishi Y, Arita N, Yamasaki M, Okano H, Hara M, Miyake J. 2002. Evaluation of in vitro proliferative activity of human fetal neural stem/progenitor cells using indirect measurements of viable cells based on cellular metabolic activity. J Neurosci Res 69:869–879.

Kirik D, Annett LE, Burger C, Muzyczka N, Mandel RJ, Bjorklund A. 2003. Nigrostriatal α-synucleinopathy induced by viral vector-mediated overexpression of human α-synuclein: a new primate model of Parkinson's disease. Proc Natl Acad Sci USA 100:2884–2889.

Koda M, Murakami M, Ino H, Yoshinaga K, Ikeda O, Hashimoto M, Yamazaki M, Nakayama C, Moriya H. 2002. Brain-derived neurotrophic factor suppresses delayed apoptosis of oligodendrocytes after spinal cord injury in rats. J Neurotrauma 19:777–785.

Levi AD, Dancausse H, Li X, Duncan S, Horkey L, Oliviera M. 2002. Peripheral nerve grafts promoting central nervous system regeneration after spinal cord injury in the primate. J Neurosurg 96: 197–205.

Li Y, Field PM, Raisman G. 1997. Repair of adult rat corticospinal tract by transplants of olfactory ensheathing cells. Science 277:2000–2002.

Liu S, Aghakhani N, Boisset N, Said G, Tadie M. 2001. Innervation of the caudal denervated ventral roots and their target muscles by the rostral spinal motoneurons after implanting a nerve autograft in spinal cord-injured adult marmosets. J Neurosurg 94:82–90.

Liu Y, Kim D, Himes BT, Chow SY, Schallert T, Murray M, Tessler A, Fischer I. 1999. Transplants of fibroblasts genetically modified to express BDNF promote regeneration of adult rat rubrospinal axons and recovery of forelimb function. J Neurosci 19:4370–4387.

Mansfield K. 2003. Marmoset models commonly used in biomedical research. Comp Med 53:161–172.

McDonald JW, Liu XZ, Qu Y, Liu S, Mickey SK, Turetsky D, Gottlieb DI, Choi DW. 1999. Transplanted embryonic stem cells survive, differentiate and promote recovery in injured rat spinal cord. Nat Med 5:1410–1412.

Metz GA, Curt A, van de Meent H, Klusman I, Schwab ME, Dietz V. 2000. Validation of the weight-drop contusion model in rats: a comparative study of human spinal cord injury. J Neurotrauma 17:1–17.

Miyoshi Y, Date I, Ohmoto T. 1995. Three-dimensional morphological study of microvascular regeneration in cavity wall of the rat cerebral cortex using the scanning electron microscope: implications for delayed neural grafting into brain cavities. Exp Neurol 131: 69–82.

AQ4

Miyoshi Y, Date I, Ohmoto T. 1995. Neovascularization of rat fetal neocortical grafts transplanted into a previously prepared cavity in the cerebral cortex: a three-dimensional morphological study using the scanning electron microscope. Brain Res 681:131–40.

AQ4

Mizuguchi R, Sugimori M, Takebayashi H, Kosako H, Nagao M, Yoshida S, Nabeshima Y, Shimamura K, Nakafuku M. 2001. Combinatorial roles of olig2 and neurogenin2 in the coordinated induction of panneuronal and subtype-specific properties of motoneurons. Neuron 31:757–771.

Nakamura M, Houghtling RA, MacArthur L, Bayer BM, Bregman BS. 2003. Differences in cytokine expression profile between acute and secondary injury in adult rat spinal cord. Exp Neurol 184:313–325.

Namiki J, Kojima A, Tator CH. 2000. Effect of brain-derived neurotrophic factor, nerve growth factor, and neurotrophin-3 on functional recovery and regeneration after spinal cord injury in adult rats. J Neurotrauma 17:1219–1231.

Ogawa Y, Sawamoto K, Miyata T, Miyao S, Watanabe M, Nakamura M, Bregman BS, Koike M, Uchiyama Y, Toyama Y, Okano H. 2002. Transplantation of in vitro-expanded fetal neural progenitor cells results in neurogenesis and functional recovery after spinal cord contusion injury in adult rats. J Neurosci Res 69:925–933.

Ohta K, Fujimura Y, Nakamura M, Watanabe M, Yato Y. 1999. Experimental study on MRI evaluation of the course of cervical spinal cord injury. Spinal Cord 37:580–584.

Okada S, Nakamura M, Mikami Y, Shimazaki T, Mihara M, Ohsugi Y, Iwamoto Y, Yoshizaki K, Kishimoto T, Toyama Y, Okano H. 2004. Blockade of interleukin-6 receptor suppresses reactive astrogliosis and ameliorates functional recovery in experimental spinal cord injury. J Neurosci Res 76:265–276.

Okano H. 2002. Stem cell biology of the central nervous system. J Neurosci Res 69:698–707.

Okano H, Ogawa Y, Nakamura M, Kaneko S, Iwanami A, Toyama Y. 2003. Transplantation of neural stem cells into the spinal cord after injury. Semin Cell Dev Biol 379:1–8.

Olson L. 2002. Clearing a path for nerve growth. Nature 416:589–590.

Schwab ME. 2002. Repairing the injured spinal cord. Science 295:1029–1031.

Silver J, Miller JH. 2004. Regeneration beyond the glial scar. Nat Rev Neurosci 5:146–156.

Smith JP, Hicks PS, Ortiz LR, Martinez MJ, Mandler RN. 1995. Quantitative measurement of muscle strength in the mouse. J Neurosci Methods 62:15–19.

Suresh Babu R, Muthusamy R, Namasivayam A. 2000. Behavioural assessment of functional recovery after spinal cord hemisection in the bonnet monkey (Macaca radiata). J Neurol Sci 178:136–152.

Svendsen CN, ter Borg MG, Armstrong RJ, Rosser AE, Chandran S, Ostenfeld T, Caldwell MA. 1998. A new method for the rapid and long term growth of human neural precursor cells. J Neurosci Methods 85:141–152.

't Hart BA, van Meurs M, Brok HP, Massacesi L, Bauer J, Boon L, Bontrop RE, Laman JD. 2000. A new primate model for multiple sclerosis in the common marmoset. Immunol Today 21:290–297.

Taupin P, Ray J, Fischer WH, Suhr ST, Hakansson K, Grubb A, Gage FH. 2000. FGF-2-responsive neural stem cell proliferation requires CCg, a novel autocrine/paracrine cofactor. Neuron 28:385–397.

Teng YD, Lavik EB, Qu X, Park KI, Ourednik J, Zurakowski D, Langer R, Snyder EY. 2002. Functional recovery following traumatic spinal cord injury mediated by a unique polymer scaffold seeded with neural stem cells. Proc Natl Acad Sci USA 99:3024–3029.

Terashima T, Ochiishi T, Yamauchi T. 1994. Immunohistochemical detection of calcium/calmodulin-dependent protein kinase II in the spinal cord of the rat and monkey with special reference to the corticospinal tract. J Comp Neurol 340:469–479.

Tuszynski MH, Grill R, Jones LL, McKay HM, Blesch A. 2002. Spontaneous and augmented growth of axons in the primate spinal cord: effects of local injury and nerve growth factor-secreting cell grafts. J Comp Neurol 449:88–101.

Vroemen M, Aigner L, Winkler J, Weidner N. 2003. Adult neural progenitor cell grafts survival after acute spinal cord injury and integrate along axonal pathway. Eur J Neurosci 18:743–751.

Watanabe K, Nakamura M, Iwanami A, Fujita Y, Kanemura Y, Toyama Y, Okano H. 2004. Comparison between fetal spinal cord-and forebrain-derived neural stem/progenitor cells as a source of transplantation for spinal cord injury. Dev Neurosci 26 (in press).

Widenfalk J, Lundstromer K, Jubran M, Brene S, Olson L. 2001. Neurotrophic factors and receptors in the immature and adult spinal cord after mechanical injury or kainic acid. J Neurosci 21:3457–3475.

Zhou Q, Choi G, Anderson DJ. 2001. The bHLH transcription factor Olig2 promotes oligodendrocyte differentiation in collaboration with Nkx2.2. Neuron 31:791–807.

Available online at www.sciencedirect.com

SCIENCE DIRECT

Developmental Biology 275 (2004) 124–142

DEVELOPMENTAL BIOLOGY

www.elsevier.com/locate/ydbio

Retinoic-acid-concentration-dependent acquisition of neural cell identity during in vitro differentiation of mouse embryonic stem cells

Yohei Okada[a,b,c], Takuya Shimazaki[a,c], Gen Sobue[b], Hideyuki Okano[a,c,*]

[a]*Department of Physiology, Keio University School of Medicine, Shinjuku-ku, Tokyo 160-8582, Japan*
[b]*Department of Neurology, Nagoya University Graduate School of Medicine, Showa-ku, Nagoya 466-8550, Japan*
[c]*Core Research for Evolutional Science and Technology (CREST), Japan Science and Technology Agency, Kawaguchi, Saitama 332-0012, Japan*

Received for publication 11 February 2004, revised 19 July 2004, accepted 21 July 2004
Available online 8 September 2004

Abstract

Retinoic acid (RA) is one of the most important morphogens, and its embryonic distribution correlates with neural differentiation and positional specification in the developing central nervous system. To investigate the concentration-dependent effects of RA on neural differentiation of mouse embryonic stem cells (ES cells), we investigated the precise expression profiles of neural and regional specific genes by ES cells aggregated into embryoid bodies (EBs) exposed to various concentrations of RA or the BMP antagonist Noggin. RA promoted both neural differentiation and caudalization in a concentration-dependent manner, and the concentration of RA was found to regulate dorso-ventral identity, i.e., higher concentrations of RA induced a dorsal phenotype, and lower concentrations of RA induced a more ventral phenotype. The induction of the more ventral phenotype was due to the higher expression level of the N-terminus of sonic hedgehog protein (Shh-N) when treated with low concentration RA, as it was abrogated by an inhibitor of Shh signaling, cyclopamine. These findings suggest that the concentration of RA strictly and simultaneously regulates the neuralization and positional specification during differentiation of mouse ES cells and that it may be possible to use it to establish a strategy for controlling the identity of ES-cell-derived neural cells.

Keywords: Embryonic stem cells; Neural differentiation; Retinoic acid; Sonic hedgehog; N-terminus of Sonic hedgehog; Positional identity; Motor neuron; Morphogen

Introduction

Embryonic stem cells (ES cells) are clonal cell lines derived from the inner cell mass (ICM) of developing blastocysts and under appropriate conditions are capable of proliferating extensively and generating various cell types derived from the three primary germ layers of the embryo in vitro. This pluripotency of ES cells provides a powerful in vitro model for investigating the mechanisms that control differentiation in early embryonic development. The basic strategy for in vitro differentiation usually adopted is to induce cell aggregation into so-called embryoid bodies (EBs) through suspension culture in nonadhesive dishes or hanging drops. Different inducing conditions during EB formation can drastically affect the proportions of the various cell types that differentiate in EBs. For example, exposure to high-concentration RA strongly drives neural induction, whereas low-concentration RA induces cardiomyocyte differentiation (Rohwedel et al., 1999). Because neural cells represent only a small percentage of cells in EBs cultured in the presence of fetal bovine serum (FBS) and the absence of an exogenous inducer, efficient generation of neural cells requires an additional inductive stimulus or other differentiation method.

There are two major strategies for generating neural cells from mouse ES cells: EB formation and serum-free direct induction. The former includes treatment with high-concentration RA (Bain et al., 1995; Fraichard et al., 1995; Strubing et al., 1995), which has been shown to promote

* Corresponding author. Department of Physiology, Keio University, School of Medicine, 35 Shinanomachi, Shinjuku-ku, Tokyo 160-8582, Japan. Fax: +81 3 3357 5445.
E-mail address: hidokano@sc.itc.keio.ac.jp (H. Okano).

0012-1606/$ - see front matter © 2004 Elsevier Inc. All rights reserved.
doi:10.1016/j.ydbio.2004.07.038

neural gene expression and repress mesodermal gene expression (Bain et al., 1996), and serum-free culture after EB formation, which enables selection of neural cells (Okabe et al., 1996). Direct induction methods consist of a co-culture system with stromal cell line PA6 as a neural inducer that has been found to have stromal-cell-derived inducing activity (SDIA) (Kawasaki et al., 2000), a low-cell-density neural stem cell (NSC) culture (neurosphere culture) with growth factors (Tropepe et al., 2001), and an adherent monolayer culture method (Ying et al., 2003).

Sequences of events leading to lineage commitment similar to those in vivo are often observed with all of these culture strategies, and, for example, exposure to Noggin or other manipulations that inhibit bone morphogenetic protein (BMPs) signaling, which blocks neural differentiation in the early development, facilitates neural differentiation of ES cells also in vitro (Finley et al., 1999; Gratsch and O'Shea, 2002; Kawasaki et al., 2000; Tropepe et al., 2001).

During the development of the mammalian central nervous system (CNS), the differentiation properties of neural stem cells (NSCs) vary depending on the stage at which they are generated (temporal identity) and their location (positional identity). These properties define the induction and sequential rounds of neurogenesis and gliogenesis, which seem to be regulated by both intrinsic and extrinsic factors, and limit their plasticity (Temple, 2001). Depending on their location, their differentiation is usually regulated by secreting signals that modulate the rostrocaudal or dorso-ventral axis of the body and by regional cues that define the borders of each CNS segment (Hitoshi et al., 2002; Temple, 2001). In view of these characteristics of NSCs, the temporal and positional identity of NSCs derived from ES cells may be controlled in vitro by the conditions under which they differentiate, the same as specification in vivo. Indeed, much interest has been focused on the generation of specific types of neurons or neural progenitors from ES cells by producing these identities with inductive signals, such as fibroblast growth factor (FGF) 8 and Shh, or with SDIA for dopaminergic neurons (Kawasaki et al., 2000, 2002; Kim et al., 2002; Lee et al., 2000; Ying et al., 2003), RA and Shh for motor neurons (Renoncourt et al., 1998; Wichterle et al., 2002), and a combination of SDIA and BMPs for dorsal and neural-crest-derived cells (Mizuseki et al., 2003).

RA is well known as the biologically active form of vitamin A and has been shown to play an important role during embryogenesis (Ross et al., 2000). RA influences neural development in the early stage of CNS development and is required to establish patterned territories of cell groups, which, for example, has been observed in rostrocaudal axis formation, according to the distribution of RA in experiments on *Xenopus* (Blumberg et al., 1997; Sive et al., 1990) and mice (Kessel, 1992; Kessel and Gruss, 1991; Marshall et al., 1992). For these reasons, RA has been thought to be one of the most important extrinsic inductive signals that can be used for neural differentiation of mouse ES cells in vitro. However, its overall effects have yet to be clearly identified, and precise analysis of alterations of gene expression caused by RA treatment should be useful for establishing proper culture protocols for the differentiation of ES cells. In the present study, we demonstrated that RA promotes neural differentiation and caudalization in a concentration-dependent manner, and that the concentration of RA affects dorso-ventral positional identity, by determining the precise gene expression profiles during differentiation of ES cells.

Materials and methods

ES cell culture

Mouse ES cells (EB3) were maintained and used for induction. ES cells were grown on gelatin-coated (0.1%) tissue culture dishes in standard ES-cell culture medium containing GMEM (Sigma G6148) supplemented with 10% FBS, glutamine (2 mM), nonessential amino acids (0.1 mM), sodium pyruvate (1 mM), 2-mercaptoethanol (2-ME) (0.1 mM), sodium bicarbonate (3 mM), HEPES (5 mM), and mLIF. EB3 is a subline derived from E14tg2a ES cells (Hooper et al., 1987) that was generated by targeted integration of Oct3/4-IRES-BSD-pA vector (Niwa et al., 2000) into the *Oct3/4* allele, and it was maintained in the medium containing 10 μg/ml blasticidin S to eliminate differentiated ES cells.

Differentiation of ES cells

For embryoid body (EB) formation, ES cells were detached and dissociated into single cells with 0.25% trypsin–EDTA and then plated onto a bacteriological dish (Kord-Valmark™) in 10 ml of αMEM (Gibco 11900-024) supplemented with 10% FBS, sodium bicarbonate (3 mM), and 0.1 mM 2-ME (EB medium) at a density of 5×10^4 cells/ml. On day 2, various concentrations of all-*trans*-retinoic acid (RA: Sigma R 2625) were added to the culture medium (2−/4+ protocol). RA was reconstituted with 100% ethanol to prepare a stock solution. It should be noted that the effective RA concentrations at which ES cells grow into EBs may be considerably higher than those indicated in the text, because FBS contains significant levels of RA. Furthermore, cells within EBs may produce endogenous RA, possibly as a secondary effect of the initially added RA. However, we used conditions in which FBS did not contain exogenous RA as a negative control (stated control in the figures), and evaluated the results in terms of relative concentrations of RA. Recombinant mouse Sonic Hedgehog (Shh) protein (amino-teminal peptide) (Shh-N; R&D Systems Inc., 461-SH) and cyclopamine (0.1 μM, 1 μM, Toronto Research Chemicals Inc., C988400) were also added on day 2 of the experiment. For Noggin treatment, 10% (v/v) culture supernatant of Cos7

cells transfected with *Xenopus* Noggin/MC BOS (a gift of Y. Takahashi) (Kohyama et al., 2001; Tonegawa and Takahashi, 1998) (xNoggin conditioned medium) was added.

EBs were collected at day 6 of culture and allowed to settle to the bottom of the tube for a few minutes. The cells were then washed once with PBS and incubated with 0.25% trypsin–EDTA for 5 min at 37°C. The enzymatic reaction was quenched by addition of an equal volume of EB medium, and the cells were dissociated with a transfer pipette by triturating 30 times. The cells were then washed twice with serum-free αMEM and resuspended in Media hormone mix (MHM) medium, which contains DMEM/F-12 (1:1) (Gibco 12100-046, 21700-075), glucose (0.6%), glutamine (2 mM), sodium bicarbonate (3 mM), HEPES (5 mM), insulin (25 μg/ml), transferrin (100 μg/ml), progesterone (20 nM), sodium selenate (30 ng), and putrescine (60 nM) (all from Sigma except for DMEM/F-12) as described previously (Shimazaki et al., 2001). The dissociated EBs were plated on poly-L-ornithine/fibronectin-coated 10-mm cover glasses (Matsunami) at a cell density of 1.6×10^5 cells/0.75 cm^2 on a 48-well culture plate (Coaster) and allowed to differentiate for 24 h.

To clarify the effects of RA added at different points in time or of exposure for different periods of culture, ES cells were differentiated into EBs based on 2−/2+/2−, 2−/2+/2+ and 4−/4+ protocols (Suppl. Fig. 1). In the 2−/2+/2− and 2−/2+/2+ protocol, various concentrations of RA were added on day 2, and on day 4 the culture medium was replaced with freshly prepared medium containing the same concentrations of RA (2−/2+/2+ protocol) or no RA (2−/2+/2− protocol). In the 4−/4+ protocol, various concentrations of RA were added to the culture medium on day 4. Total RNA was isolated at day 0, 2, 4, 6, and 8 and processed for RT-PCR analysis.

Immunocytochemistry

Dissociated EBs were cultured for 24 h and fixed with 4% paraformaldehyde for 20 min at room temperature. The cells were rinsed with PBS twice and pretreated with PBS containing 0.3% Triton -X100 for 5 min at room temperature. After blocking in TNB buffer (Provided by NEN™ Life Science Products, Inc.) for 1 h at room temperature, the cells were incubated at 4°C overnight with the following antibodies: anti-Nestin (Rat-401, mouse IgG, 1:200), anti-Islet-1/2 (40.2D6, mouse IgG, 1:500), anti-Lim3 (67.4E12, mouse IgG, 1:1000), anti-HB9 (81.5C10, mouse IgG, 1:100), anti-Otx1 (Otx-5F5, mouse IgG, 1:500000), anti-Nkx2.2 (74.5A5, mouse IgG, 1:5000), anti-Pax7 (mouse IgG, 1:5000) (Developmental Studies of Hybridoma Bank: DSHB), anti-βIII-tubulin (mouse IgG, 1:1000, Sigma T8660), anti-Olig2 (rabbit IgG, 1:30000) (Mizuguchi et al., 2001; Takebayashi et al., 2000), anti-Phox2b (rabbit IgG, 1:25000) (Pattyn et al., 1997), anti-Nkx6.1 (Ab174.3, rabbit IgG., 1:200000) (Jensen et al., 1996), anti-Group B1 Sox [Sox1/(2)/3] (rabbit IgG, 1:10000) (Tanaka et al., unpublished). Anti-Group B1 Sox [Sox1/(2)/3] antibody is weakly reactive with Sox2, which is expressed not only by the neural primordium but by undifferentiated ES cells, and with Sox1 and Sox3 (with preference for Sox1 and Sox3 over Sox2). However, as all Group B1 Sox genes are expressed in neural primordium (Wood and Episkopou, 1999), we used this antibody to detect neural progenitors, by determining the immunostaining conditions under which undifferentiated ES cells, which were used as a negative control, did not stain (data not shown). Antigen retrieval was accomplished by incubating the samples in the boiled PBS for 10 min for anti-Isl-1/2 and anti-Lim3, in boiled Target Retrieval Solution (DAKO) for 10 min for anti-Nkx2.2, or in 1 N HCl at 30°C for 15 min for anti-Pax7. After washing with PBS three times, the cells were incubated for 1 h at room temperature with secondary antibodies conjugated with Alexa 488 or Alexa 568 (Molecular Probes). For anti-Islet1/2, anti-Lim3, anti-HB9, anti-Olig2, anti-Phox2b, anti-Otx1, anti-Nkx2.2, anti-Pax7, and anti-Nkx6.1 staining, we used biotinylated secondary antibodies (Jackson Immunoresearch Laboratory, Inc.) after exposure to 1% H_2O_2 for 15 min at room temperature to inactivate endogenous peroxidase. The signals were then enhanced with streptavidin-HRP (SA-HRP), followed by TSA™ Fluorescein System (NEN™ Life Science Products, Inc.). After washing with PBS, the samples were mounted on slides and examined with a universal fluorescence microscope (Axiophot 2, Carl Zeiss) and a confocal laser scanning microscope (LSM510, Carl Zeiss). The nuclei of all samples were stained with hoechst33342 (1 μg/ml, Sigma B2261). For statistical analysis, at least 200 cells per cover glass were examined, and the numbers of cells that had immunoreacted with each antibody were counted and expressed as a percentage of the total number of cells whose nuclei stained with hoechst33342. The *P* values for statistical significance (*t* test) are stated in the figure legends.

Western blot analysis

Western blot analysis was performed by the previously established method. A 20 μg protein sample of a total cell extract was run on 7.5–15% SDS-PAGE, transferred to nitrocellulose, and probed with each antibody. The blot was probed with the following antibodies: anti-Nestin (Rat-401, mouse IgG, Developmental Studies of Hybridoma Bank: DSHB), anti-βIII-tubulin (mouse IgG, Sigma T8660), anti-Glial Fibrillary Acidic Protein (GFAP) (rabbit IgG, DAKO Z0334), anti-CNPase (mouse IgG, Sigma C5922), and anti-Shh N-terminal fragment (goat IgG, Santa Cruz sc-1194). Signals were detected with HRP-conjugated secondary antibodies (Jackson Immunoresearch Laboratory, Inc.) by using an ECL kit (Amersham Biosciences). Quantitative analysis was performed with Scion Image (Scion Corpo-

ration). The amounts of proteins loaded in each slot were normalized to those of α-tubulin.

RNA isolation and RT-PCR

RT-PCR analysis of at least two independent cultures was performed in most of the experiments, and were similar results obtained. Total RNA was isolated with Trizol reagent (Invitrogen™ 15596-018) and DNase I treatment, or by the RNeasy Mini Kit (Qiagen). Total RNA (1–3 μg) was used to synthesize cDNA with 500 ng oligo-d(T)$_{12-18}$ primers. The cDNA synthesis was performed at 42°C for 50 min in a final volume of 20 μl according to the manufacturer's instructions for Superscript II RNase H$^-$ reverse transcriptase (Invitrogen™). To analyze relative expression of different mRNAs, the amount of cDNA was normalized based on the signals from ubiquitously expressed *β-actin* mRNA. The PCR was carried out by using a KOD Plus kit (Toyobo) according to the manufacturer's standard protocol in a final volume of 25 μl. Primer sequences and PCR cycling conditions will be provided upon request. To provide negative controls and exclude contamination by genomic DNA, the reverse transcriptase was omitted in the cDNA synthesis step, and the samples were subjected to the PCR reaction in the same manner with primer sets for *β-actin*, and are indicated at the bottom of each figure as RT(−). PCR products were electrophoresed in agarose gel, and bands were visualized with ethidium bromide under UV light. The identity of the PCR products was confirmed by sequencing.

Results

Differentiation potential of mouse ES cells regulated by RA

RA has been shown to be one of the most important extrinsic morphogens and precisely modulates the differentiation properties of ES cells into various cell types, including neural cells, skeletal muscle cells, adipocytes, cardiomyocytes, and vascular smooth muscle cells, in an incubation-time- and concentration-dependent manner (Rohwedel et al., 1999). To examine the concentration-dependent effects of RA on the differentiation of ES cells, we first differentiated ES cells by inducing the formation of EBs in the presence of various concentrations of RA. We also used Noggin, a secreted protein that plays a role in neural induction by inhibiting BMP-signaling (Finley et al., 1999; Gratsch and O'Shea, 2002; Kawasaki et al., 2000; Smith and Harland, 1992; Tropepe et al., 2001; Zimmerman et al., 1996), to investigate RA-independent neural differentiation. ES cells were plated onto bacteriological dishes and had been cultured for 6 days in medium containing various concentrations of RA (added on day 2) or xNoggin conditioned medium (Fig. 1), and they were analyzed by RT-PCR for markers of the three primary germ layers

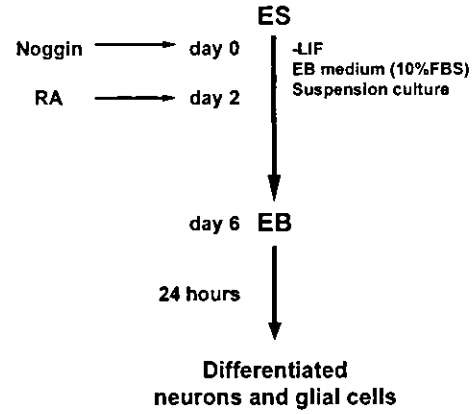

Fig. 1. Experimental protocol for differentiation of ES cells with retinoic acid (RA) or xNoggin conditioned medium. ES cells were cultured in the bacteriological dish for 6 days and formed embryoid bodies (EBs). Various concentrations of RA were added on day 2 of EB formation. Then, EBs were dissociated and differentiated on poly-L-ornithine/fibronectin-coated cover glasses.

(Fig. 2). On day2, *oct3/4*, which is a marker for undifferentiated ES cells, was expressed by both control and Noggin-treated EBs. From day 4 of EB formation onward, *oct3/4* expression was gradually down-regulated by RA in a concentration-dependent manner and in a culture period-dependent manner, and it became undetectable on day 6 under all conditions, indicating that most of the ES cells had differentiated by 6 days of EB formation. On day 6, expression of *ck-17 (cytokeratin 17)*, a marker of epidermis (McGowan and Coulombe, 1998), and expression of *ngn2*, which is expressed in neuronal progenitors (Mizuguchi et al., 2001; Novitch et al., 2001; Ross et al., 2003), were enhanced by high-concentration RA treatment (>10^{-7} M; high-RA), and thus ectodermal differentiation was promoted by exposure to high-RA. Expression of *ck-17* mRNA in undifferentiated ES cells, which also expressed *oct3/4* (Fig. 2), was also demonstrated in a previous study (Tropepe et al., 2001). In the control, Noggin, and low-RA-treated EBs, its expression coincided with expression of *oct3/4* at day 4, and was then down-regulated by day 6 along with extinction of *oct3/4*. In the high-RA-treated EBs, on the other hand, expression of *ck-17* mRNA was detected at day 4 and day 6, without expression of *oct3/4*. The expression of *ck-17* in the absence of expression of *oct3/4* can be understood as indicating promotion of epidermal differentiation in EBs treated with high-RA. Mesodermal differentiation, represented by expression of *brachyury*, which is essential for the formation and organization of mesoderm (Herrmann et al., 1990; Wilkinson et al., 1990), and expression of homeobox gene *nkx2.5*, the earliest known marker of cardiac development (Komuro and Izumo, 1993; Lints et al., 1993), were facilitated by low-concentration RA treatment (10^{-9}–10^{-8} M; low-RA). Endodermal markers, including *gata4*, expressed in primitive endoderm (Arceci et al., 1993), and *pdx1*, expressed in developing pancreas (Jonsson et al., 1994; Offield et al., 1996), were